Floating Particles

P. Singh
Department of Mechanical Engineering
New Jersey Institute of Technology
Newark, NJ 07102
Email: singhp@njit.edu

D.D. Joseph
Department of Aerospace Engineering and Mechanics
University of Minnesota
Minneapolis, MN 55455
Email: joseph@aem.umn.edu

A finite element code based on the level set and distributed Lagrange multiplier (DLM) methods is developed for simulating the motion of rigid spherical particles on two-fluid interfaces. The interface position is tracked using a level set function. The contact angle on the particle surface is assumed to be constant, even when the contact line on the particle surface moves. The fluid-particle system is treated implicitly using a combined weak formulation in which the forces and moments between the particles and fluid cancel. The governing Navier-Stokes equations are solved everywhere, including inside the particles. The flow inside the particles is forced to be a rigid body motion by a distribution of Lagrange multipliers. The Marchuk-Yanenko operator-splitting technique is used to decouple the difficulties associated with the nonlinear convection term, the incompressibility constraint, the rigid body motion constraint inside the particles and the interface motion problem.

The code is verified by performing a convergence study to show that the numerical results are independent of the mesh and time step sizes. Simulations show that a spherical particle released on a two-fluid interface can remain suspended even when it is heavier than both liquids, provided the vertical component of interfacial force balances its buoyant weight. This can happen when the sphere is hydrophobic with the lower fluid and hydrophilic with the upper fluid, as in this case the interfacial force can act against gravity. The numerically determined floating height and the interface shape are in good agreement with the analytical results for static equilibrium. Our simulations also show that when two or more particles are released along the interface they, as in experiments, form clusters due the attractive capillary force which arises due to the asymmetric interface deformation around the particles. Specifically, the heavy particles lower the interface creating depression. The particles then experience a lateral attractive force due to gravity and capillarity. The gravity force causes the particle to fall into the depression; this lowers and tilts the contact line. The lower contact line is associated with a smaller vertical component of the capillary force for a fixed angle of contact and the rotation of the contact line produces imbalance in the horizontal component. The former increases the depth to which the particles sink in the lower fluid.

1. Introduction

It is well known that the small tea leaves floating on the tea surface collect near the cup wall which is due to the formation of meniscus that rises near the wall and results in a net capillary force towards the wall. The meniscus rises near the wall because the water wets or likes the cup. If, on the other hand, the liquid does not like the cup, i.e., the meniscus falls near the cup wall, floating small particles tend to move away from the wall and towards the center of the cup. Similarly, the deformation of liquid-liquid interfaces due to floating light particles, or due to trapped heavy particles, gives rise to capillary forces on the particles which cause them to cluster, as can be seen in figure 1. The clustering of particles on interfaces is important because it modifies the interfacial properties of the two-phase system and has been used in many flotation based extraction and separation processes (Gerson, Zaijc and Ouchi (1979)). More recently, this effect has been used for the self-assembly of submicron sized particles on two-liquid interfaces (see Bowden, et al. (1997,1999), Grzybowski, et al. (2001), and references therein).

The motion of tea leaves along the interface, in the above example, is entirely due to the deformation of the meniscus near the cup wall. The clustering of particles, on the other hand, is a consequence of the interface deformation caused by neighboring particles. Specifically, when two heavy particles, hydrophobic with respect to the lower liquid, are sufficiently close to each other the deformed interface shape around the particles is not symmetric about the vertical passing through their respective centers, as the interface height between the particles is lowered due to the interfacial force which acts downwards (see figure 2a). If, on the other hand, the particles are less dense than the lower liquid and hydrophilic with respect to it, the interface height between the particles is raised due to the action of interfacial force (see figure 2b). In both of these cases, the lateral component of interfacial tension is attractive which causes the spheres to move toward each other. But, when one particle is hydrophilic and the other is hydrophobic with respect to the lower liquid, the lateral force is repulsive which causes them to move away from each other.

For convenience, in our analysis we will assume that the lower fluid is water, the upper fluid is air and the spherical particle is hydrophobic. The qualitative nature of above forces can be understood in terms of the net vertical and lateral forces, i.e., normal and tangential to the undeformed interface, acting on a sphere when the system is in a state of static equilibrium, i.e., there is no fluid or particle motion. This analysis was given first by Princen (1969), then by Rapacchietta and Neumann (1977) and Kotah, Fujita and Imazu (1992), who used the floating ball to measure contact angles.

In order to have static equilibrium, the buoyant weight of particle must be equal to the vertical component of capillary force that arises due to the deformation of the interface. If the particle density is larger than that of both fluids, the static equilibrium is possible only when the particle is hydrophobic with respect to the lower fluid and hydrophilic with the upper fluid and the vertical component of

interfacial tension is sufficiently large to balance its buoyant weight. The interface shape in this case is concave down and the net interfacial force acts against gravity.

1.1 Vertical force balance

Next, we discuss the results of vertical force balance that quantify the conditions under which an isolated floating sphere can be a state of static equilibrium. It is easy to see that the vertical component of capillary force F_C depends on the particle radius R, the surface tension coefficient γ, the filling angle θ_c and the contact angle α (see figure 3), and is given by

$$F_C = 2\pi(R\sin\theta_c)\gamma\sin[\theta_c - (\pi - \alpha)] = -2\pi(R\sin\theta_c)\gamma\sin(\theta_c + \alpha). \quad (1)$$

The above expression holds for both the hydrophobic and hydrophilic cases. In the former case the capillary force F_C acts upwards against gravity and in the latter case it acts downwards.

It is worth noting that if $\theta_C + \alpha > \pi$, F_C is positive or acts against gravity, and if $\theta_C + \alpha < \pi$, it is negative. Therefore, if a particle is heavier than water and hydrophobic, it can float only when $\theta_C + \alpha > \pi$ and F_C is equal to its buoyant weight. Also notice that for $\alpha = 3\pi/4$ and $\theta_C = \pi/4$, the force F_C is zero and there is no interface deformation (see figure 4). It increases, when θ_C is increased from $\pi/4$ and reaches its maximum value at $\theta_C \approx 1.9$ and then decreases with increasing θ_C. On the other hand, when the contact angle is π, F_C is always non-negative and its maximum value is for $\theta_C = \pi/2$, i.e., the sphere half immersed in the lower liquid. The buoyant weight of the particle, of course, also changes with θ_C.

For static equilibrium, the sum of capillary force and the vertical resultant of pressure around the sphere must be equal to the particle weight:

$$F_C + F_p = \frac{4}{3}\pi\rho_p R^3 g. \quad (2)$$

where ρ_p is the particle density and F_p is the vertical resultant of pressure around the sphere (see figure 2). By integrating the contribution of pressure to force on the sphere surface, we can write F_p as

$$F_p = \rho_l g\pi R^3\left(\frac{2}{3} - \cos\theta_c + \frac{1}{3}\cos^3\theta_c\right) + \rho_a g\pi R^3\left(\frac{2}{3} + \cos\theta_c - \frac{1}{3}\cos^3\theta_c\right) - (\rho_l - \rho_a)gh_2\pi R^2\sin^2\theta_c. \quad (3)$$

where h_2 is the meniscus height, which rises or falls, and ρ_l and ρ_a are the densities of the lower and upper fluids, respectively. Using the fact that $V = \frac{4}{3}\pi R^3$ is the volume of the sphere,

$V_w = \pi R^3(\frac{2}{3} - \cos\theta_c + \frac{1}{3}\cos^3\theta_c)$ is the volume of the sphere immersed in the water and $A = \pi R^2 \sin^2\theta_c$ is the area of the ring of contact, we can rewrite (3) as:

$$F_p = \rho_l g v + \rho_a g(V - V_w) - (\rho_l - \rho_a) g h_2 A \tag{4}$$

The first two terms on the right hand side are in agreement with Archimedes' principle, while the term $(\rho_l - \rho_a) g h_2 A$ accounts for the meniscus effect. When a meniscus is present, the buoyancy calculated by Archimedes' principle $\rho_l g v + \rho_a g(V - v)$ not only lifts the sphere, but also the fluid in the meniscus. Hence, we need to subtract the weight of the lifted fluid from $\rho_l g v + \rho_a g(V - v)$ to get the buoyancy force acting on the sphere. Expression (4) implies that the volume of the lifted fluid is $h_2 A$.

Inserting (1) and (3) into (2), we can write the dimensionless vertical force balance as

$$\begin{aligned} \sin\theta_c \sin(\theta_c + \alpha) = -\frac{1}{2} B[\frac{4}{3}\psi_1 - (\frac{2}{3} - \cos\theta_c + \frac{1}{3}\cos^3\theta_c) - \\ \psi_2(\frac{2}{3} + \cos\theta_c - \frac{1}{3}\cos^3\theta_c) + (1 - \psi_2)(\cos\theta_1 - \cos\theta_c)\sin^2\theta_c] \end{aligned} \tag{5}$$

where $B = \rho_l R^2 g/\gamma$ is the Bond number and $\psi_1 = \rho_p/\rho_l$ and $\psi_2 = \rho_a/\rho_l$ are the dimensionless density parameters.

Notice that the left side of (5), and thus also the right side, lie in the range $-1 \le \sin\theta_C \sin(\theta_C + \alpha) \le 1$. Obviously, (5) cannot be solved if B is too large which may be the case when the particle is too heavy or too large. Also, for a suspended hydrophobic heavy particle $\sin(\theta_C + \alpha)$ must be negative or $\theta_C + \alpha > \pi$. This is required because, as noted before, the interfacial force acts at an angle of $\theta_C + \alpha - \pi$ from the horizontal. Therefore, it acts against gravity only when $\theta_C + \alpha - \pi$ is positive, otherwise it acts in the same direction as gravity. For example, if $\alpha = 3\pi/4$, for a heavy particle to float $\theta_C > \pi/4$.

It is noteworthy that as R approaches zero, the interfacial force, which varies linearly with R, dominates the buoyant weight of the particles which varies as R^3. In this limit, since $\rho_p R^2 g/\gamma \to 0$, the right hand side of (5) is zero and thus $\sin(\alpha + \theta_C) \approx 0$ or $\theta_C \approx \pi - \alpha$. We may therefore conclude that small particles can be suspended along fluid surfaces without causing significant interfacial deformation no matter how heavy they are. Krahshesky, et al. (1992, 1993) have noted that for particles floating on water this limit is approximately reached when their diameter is 10 μm. Consequently, the lateral particle-particle attraction force, which arises due to interface deformation, is also insignificant when the particle diameter is smaller than 10 μm.

Even though the above result for small particles was obtained using the static equilibrium equations for spheres, it is easy to see that it is also true for particles of other shapes, including those containing flat surfaces. It, in general, implies that the floating height of a small particle must be such that the vertical component of interfacial force acting on it is zero, as its weight is negligible, which is achieved when there is negligible interface deformation. For spherical particles, this height is a function of the contact angle and nothing but the zero of the transcendental function in (1). For example, if $\alpha = 3\pi/4$, a small sphere will float with $\theta_C \approx \pi/4$. It also allows us to make the following interesting observation. If the particle surface consists of straight planes, e.g., a cube settling with its four sides vertical, the interface deformation, which strictly depends on the contact angle, cannot change when its floating height changes. The vertical component of interfacial force is therefore also independent of the floating height. This implies that a small hydrophobic cube must float such that the interface is near the edges of bottom plane, i.e., there is a negligible penetration of the lower liquid, because otherwise the interfacial deformation, and thus also the vertical interfacial force, cannot be negligible. The interfacial deformation and force, as noted earlier, depend only on the normal to the particle surface. This argument assumes that the contact angle on the particle surface remains fixed and that when the contact line is along an edge the vertical interfacial force can take any value, between the values corresponding to the two surfaces, required for equilibrium without noticeable movement of the contact line. Also note that for particles containing flat surfaces and sharp corners the interfacial force as well as the interfacial deformation change suddenly when the contact line moves from one flat surface to another, as the direction of the normal to the surface changes suddenly.

The above statement regarding a sudden change in the interfacial force around corners is true even for large heavy particles. This was demonstrated in recent experiments of Singh, Joseph, Wang and Bai (2003) where it was shown that for a cylinder floating such that its top flat surface is exposed to the air and the curved side and the bottom are immersed, the contact line remains at the corner for a wide range cylinder weights. The cylinder weight was changed by adding heavy metal balls into a conical cavity on the top surface. This demonstrates that the vertical interfacial force adjusts to balance the increased particle weight while the contact line remains "trapped" at the corner.

This was demonstrated in recent experiments reported in Singh, Joseph, Wang and Bai (2003) where it was shown that the contact line remains "trapped" at the corner even when the weight of a floating cylinder is changed by adding heavy metal balls into a conical cavity on its top surface. Specifically, they found that for a cylinder floating such that it is almost completely immersed in the water, except its top flat surface, the contact line remains at corner for a wide range cylinder weights.

Finally, we note that when particles are partially immersed in a thin liquid film, and their weight is supported by the substrate below, the interface deformation can be significant even for small particles

because the above restriction of negligible interface deformation is not applicable in this case. In fact, Kralchevsky and Nagayama (2000) have shown that in thin films the particle-particle attraction force increases with decreasing particle size.

1.2 Horizontal force balance and particle clustering

The deformation of a fluid-fluid interface due to floating or trapped particles gives rise to lateral capillary forces exerted on the particles. A simple explanation is given in figure 2. A heavier-than-liquid particle will fall down a downward sloping meniscus while an upwardly buoyant particle will rise.

There are several ways to isolate the effects of capillarity uninfluenced by gravity. Poynting and Thompson (1913) investigated the capillary effect by considering two vertical plates immersed in a liquid, the space between the plates is a two dimensional capillary tube. If the plates are hydrophobic, the level in the capillary gap sinks below the liquid outside; if the plates are hydrophilic the levels will rise. Their argument about the nature of horizontal forces on the plates is given in the caption of figure 5. Repulsion between particles with different wetting properties is rather short range because it stops when the meniscus between particles gets flat.

Another way to take away the effects of gravity is to support the particles on a substrate. In this case the horizontal forces are due to capillary effects alone. Katoh, Fujita and Imazu (1992) studied the motion of a particle floating on a liquid meniscus surface which could be interpreted as motion on a substrate because the foaming phlystyrol particles used by them are an order of magnitude lighter than water, and minimize the effects of gravity compared to capillarity. Their experimental results are completely consistent with the predictions of Poynting and Thompson: when the sphere and the wall are alike with respect to wetting; say both are hydrophobic or hydrophilic, the wall and sphere attracts; when they are unlike the sphere and wall repel.

Despite the well-established importance of the capillary meniscus forces there are only a few theoretical works devoted to them. Nicolson (1949) was the first to derive an analytical expression for the capillary force between two floating bubbles by using the superposition of approximation to solve the Laplace equation of capillarity. A similar approximate method was applied by Chan et al. (1981) to floating spheres and horizontal cylinders. For horizontal cylinders the alternative approaches were proposed by Gifford and Scriven (1971) and by Fortes (1982). The theoretical works are based on solutions of the Laplace equations for capillary menisci of translational or rotational symmetry, where the Laplace equation reduces to an ordinary differential equation.

For the case where the meniscus slope and the particle size are small, the Laplace equation for the interface shape was solved using bipolar coordinates by Krahshesky, et al. (1992, 1993). This solution

provides expressions for calculating the capillary meniscus force between two vertical cylinders, between two spheres partially immersed in a liquid layer and between a vertical cylinder and a sphere. Specifically, Kralchevsky and Nagayama have shown that the lateral force F_l acting on the particles of radii of R_1 and R_2 separated by distance L is equal in magnitude and opposite in sign and is given by

$$F_l = -2\pi Q_1 Q_2 q K_1(qL)\left[1 + O(q^2 R_k^2\right] \text{ when } L >> r_k.$$

Here $r_k = R_k \sin(\theta_c)$, k=1, 2 are the radii of the two contact lines as shown in figure 3, $Q_k = r_k \sin(\psi_k)$, where ψ_k is the interface slope with the horizontal plane at the point of contact, $q = \sqrt{(\rho_1 - \rho_p)g/\gamma}$ is the inverse of the capillary length, $K_1(x)$ is the modified Bessel function of the first order. Expression (6) is valid for particles much smaller than the capillary length. A review of this approach was given in a recent article by Kralchevsky and Nagayama (2000).

It is worth noting that since the interface curvature decreases with increasing distance from the particle, i.e., the surface becomes flatter, we may define a region of influence around the suspended particle within which the capillary force on another particle, due to interface deformation, is not small. When a suspended particle is within the region of influence of another particle, it will move along the interface due to the lateral component of the interfacial force (see figure 2).

The above static equilibrium analysis is useful for determining the parameter values for which the particles can remain trapped on two-fluid interfaces, as well as the sign and magnitude of forces that act between two suspended particles, but to understand the actual motion of particles on the interface we must solve the equations of motion. Since the governing equations are complex, the dynamic behavior of fluid particles is not well understood. Gifford and Scriven (1971) note that "casual observations… show that floating needles and many other sorts of particles do indeed come together with astonishing acceleration. The unsteady flow fields that are generated challenge analysis by both experiment and theory. They will have to be understood before the common-place 'capillary attraction' can be more than a mere label, so far as dynamic processes are concerned."

To simulate the motion of rigid particles trapped on a two-fluid interface, we must solve the governing mass and momentum conservation equations for the two fluids, compute the forces acting on the particles and then move them according to the net force acting on them. This is clearly a difficult numerical task because the interface shape changes in response to the fluid motion and across the interface the fluid properties change suddenly and an interfacial force acts between the two fluids.

In addition, we must prescribe the contact angle for the contact line on the particle surface when the particle or the interface near the particle moves. In this study we will assume that the dynamic contact angle is the same as the static contact angle. This enforcement of the contact angle on the particle surface causes the contact line to move which may be described as a capillary induced motion of the contact line

due to a prescribed contact angle (see Friedrichs and Guceri (1993) and Sussman (2001) and references therein). This motion of the contact line on the particle surface, however, is in conflict with the no slip condition for viscous fluids (see Dussan and Davis (1974), Dussan (1976) and Kistler and Scriven (1993) and references therein). But, since the fluid velocity on the particle surface is the same as that of the particle, the contact line cannot move unless the contact angle condition is used. An alternative approach used in some studies is to use a slip boundary condition in a small neighborhood of the contact line (see Friedrichs and Guceri (1993) and Kamal, Goyal and Chu (1988) and references therein).

In this work the level set method is used to track the interface (see Osher and Sethian (1988), Sussman, Smereka and Osher (1994), Pillaipakkam and Singh (2001), Sussman (2001)). The level set method works efficiently on a regular fixed grid and is compatible with the distributed Lagrange multiplier method (DLM) which will be used to track the motion of rigid particles (see Glowinski, Pan, Hesla and Joseph (1999) and Singh, Joseph, Hesla, Glowinski and Pan (2000)). The DLM method also works efficiently on regular fixed grids. It is worth noting that there are several other numerical approaches available for tracking the interface between two immiscible liquids, e.g., the surface tracking method (Unverdi and Tryggvason (1992)), the volume of fluid method (Hirt and Nichlos (1981)), the moving grid methods (Glowinski, Tallec, Ravachol and Tsikkinis (1992)) and the mapping method (Ryskin and Leal (1984)).

In the level set method, the interface position is not explicitly tracked, but is defined to be the zero level set of a smooth function ϕ, which is assumed to be the signed distance from the interface. In order to track the interface, the level set function is advected according the velocity field. One of the attractive features of this approach is that the method does not require any special treatment when a front splits into two or when two fronts merge.

In our numerical scheme the Marchuk-Yanenko operator splitting technique is used to decouple the difficulties associated with the incompressibility constraint, the nonlinear convection term, the rigid body motion constraint and the interface motion. The operator-splitting gives rise to the following four sub-problems: a L^2 projection problem for the velocity and the pressure; a nonlinear advection-diffusion problem for the velocity; a distributed Lagrange multiplier problem that forces rigid body motion within the particles; and an advection problem for the interface.

A small number of theoretical studies have looked at the drag and diffusion coefficient of a spherical particle attached to a fluid interface (Brenner and Leal (1978, 1982); Goldman, Cox and Brenner (1967); Schneider, O'Neill and Brenner (1973); Majumdar, O'Neill and Brenner (1974) and Wakiga (1957); Redoev, Nedjalkov and Djakovich (1992); Danov, Aust, Durst and Lange (1995)).

The only experimental determination of drag coefficients for particles of any size were determined by Petkov, et al. (1995) for large particles of sub-millimeter radius by measuring the particle velocity under the action of a well defined external force. They showed that the capillary interactions are quite strong and very long range. Accelerations, which are very great under many conditions of interest, have not been studied before.

The outline of the paper is as follows. In the next section we will state the governing equations for the fluids and the particles, briefly describe the level set and distributed Lagrange multiplier approaches and present our finite element method. In section 3, we will discuss the convergence study that shows that the numerical results are independent of the mesh size as well as the time step size and present results for the transient motion of particles along two-fluid interfaces.

2. Governing Equations

In our numerical studies of particle motion along two-fluid interfaces we will assume that the fluids are immiscible and Newtonian. The particles are assumed to be rigid and spherical. Let us denote the domain containing the liquid and N particles by Ω, the interior of the ith particle by $P_i(t)$ and the domain boundary by Γ. The governing mass and momentum conservation equations for the fluid phases can be written as

$$\rho_L \left[\frac{\partial \mathbf{u}}{\partial t} + \mathbf{u}.\nabla \mathbf{u} \right] = \rho_L \mathbf{g} - \nabla p + \nabla.\boldsymbol{\sigma} + \gamma \kappa \delta(\phi)\, \mathbf{n} \qquad \text{in } \Omega \backslash \overline{P(t)}$$

$$\nabla \cdot \mathbf{u} = 0 \qquad \text{in } \Omega \backslash \overline{P(t)} \qquad (6)$$

$$\mathbf{u} = \mathbf{u}_L \qquad \text{on } \Gamma \qquad (7)$$

$$\mathbf{u} = \mathbf{U} + \omega \times \mathbf{r} \qquad \text{on } \partial P(t) \qquad (8)$$

with the extra stress tensor $\boldsymbol{\sigma} = 2\eta\mathbf{D}$, ρ_L is the fluid density which is different for the two fluids, p is the pressure, **D** is the symmetric part of the velocity gradient tensor, $\delta(.)$ is the Dirac delta function, **n** is the outer normal at the interface, γ is the surface tension, κ is the surface curvature, ϕ is the distance from interface and η is the viscosity which is different for the two fluids. The surface tension force acts only along the interface.

The particle velocity **U** and angular velocity ω are governed by

$$M\frac{d\mathbf{U}}{dt} = M\mathbf{g} + \mathbf{F}$$

$$I\frac{d\boldsymbol{\omega}}{dt} = \mathbf{T} \qquad (9)$$

$$\mathbf{U}|_{t=0} = \mathbf{U}_0$$

$$\boldsymbol{\omega}|_{t=0} = \boldsymbol{\omega}_0 \qquad (10)$$

where M and I are the mass and moment of inertia of the particle, and $\mathbf{F} = \oint(-p\mathbf{I} + \boldsymbol{\sigma}).\mathbf{n}\, ds$ and $\mathbf{T} = \oint(\mathbf{x} - \mathbf{X}) \times [(-p\mathbf{I} + \boldsymbol{\sigma}).\mathbf{n}]\, ds$ are the force and torque acting on the particle, respectively. Here $\mathbf{X}$ is the center of particle and the integral is over the particle surface. The particle density will be denoted by ρ_P.

2.1 Particle Motion: The motion of particles is tracked using a distributed Lagrange multiplier method (DLM) (see Glowinski, et al. (1999) and Singh, et al. (2000)). One of the key features of the DLM method is that the fluid-particle system is treated implicitly by using a combined weak formulation where the forces and moments between the particles and fluid cancel, as they are internal to the combined system. The flow inside the particles is forced to be a rigid body motion using the distributed Lagrange multiplier method. This multiplier represents the additional body force per unit volume needed to maintain rigid-body motion inside the particle boundary, and is analogous to the pressure in incompressible fluid flow, whose gradient is the force needed to maintain the constraint of incompressibility.

2.2 Interface Tracking: The interface position in our code is tracked by using the level-set method see Osher and Sethian (1988), Sussman, et al. (1994), Pillaipakkam and Singh (2001), Sussman (2001)). The key idea in this method is to define a scalar variable ϕ, which is equal to the distance from interface, and to advect it with the local velocity, i.e.,

$$\frac{\partial \phi}{\partial t} + \mathbf{u}.\nabla\phi = 0\,. \qquad (11)$$

As ϕ is a smooth function, it is relatively easy to numerically solve the above equation to update the interface position. In our implementation, it is assumed to be negative for the upper fluid, positive for the lower fluid and zero along the interface. The method also allows us to enforce the contact angle on the rigid particle surfaces and it is relatively easy to implement it in both two and three dimensions.

The contact angle boundary condition on the particle surface which requires that $\mathbf{n}.\mathbf{n}_\phi = \cos(\alpha)$, where $\mathbf{n}$ is the unit outer normal on the particle surface and $\mathbf{n}_\phi = \frac{\nabla\phi}{|\nabla\phi|}$ is normal to the interface, is enforced using the approach described in Sussman (2001). Sussman used this approach to prescribe the contact angle on a stationary flat wall by extending ϕ to the "outside" of the fluid domain. In this article the same approach is used to prescribe the contact angle of the two-fluid interface on the surface of a moving sphere. Let us define $\mathbf{t}$ and $\mathbf{n}_2$ as

$$\mathbf{t} = \frac{\mathbf{n}_\phi \times \mathbf{n}}{|\mathbf{n}_\phi \times \mathbf{n}|}, \mathbf{n}_2 = \frac{\mathbf{t} \times \mathbf{n}}{|\mathbf{t} \times \mathbf{n}|}.$$

Notice that $\mathbf{t}$ is tangent to the contact line, and thus $\mathbf{n}_2$ is orthogonal to the contact line and lies in the tangent plane of the particle surface (see figure 6b). The next step is to construct a unit vector $\mathbf{u}_{ex}$ which is tangent to the interface with contact angle α, points inwards, and lies in the plane formed by $\mathbf{n}$ and $\mathbf{n}_2$. It is easy to verify that $\mathbf{u}_{ex}$ depends on $c = \mathbf{n}_\phi.\mathbf{n}_2$ and is given by

$$\mathbf{u}_{ex} = \begin{cases} \dfrac{\mathbf{n} - \cot(\pi - \alpha)\mathbf{n}_2}{|\mathbf{n} - \cot(\pi - \alpha)\mathbf{n}_2|} & \text{if } c < 0 \\ \dfrac{\mathbf{n} + \cot(\pi - \alpha)\mathbf{n}_2}{|\mathbf{n} + \cot(\pi - \alpha)\mathbf{n}_2|} & \text{if } c > 0 \\ \mathbf{n} & \text{if } c = 0 \end{cases} \qquad (12)$$

To enforce the prescribed contact angle condition on the particle surfaces, ϕ is extended inside particles and on their surfaces by solving

$$\frac{\partial \phi}{\partial t} + \mathbf{u_{ex}}.\nabla\phi = 0\,. \qquad (13)$$

In other words, for all nodes inside and on the particle surface the above equation is used to modify ϕ. The resulting extended level set function satisfies the contact angle condition on the particle surface.

It is worth noting that the contact line on the particle surface moves when the contact angle condition is enforced using (14). This approach has been used in many past numerical studies of problems involving moving contact lines (see Friedrichs and Guceri (1993) and Sussman (2001) and references therein). For example, in the injection molding problems this approach has been used to track the motion of liquid front advancing into empty molds.

Clearly, this motion of the contact line on the particle surface is in conflict with the noslip condition for viscous fluids (see Dussan and Davis (1974), Dussan (1976) and Kistler and Scriven (1993) and references therein). However, if the contact line position on the particle surface is not updated using the contact angle condition, the contact line cannot move because the fluid velocity on the particle surface is the same as that of the particle. This could be called the capillary induced motion of the contact due to a prescribed contact angle. The no slip condition is satisfied before and after the contact line moves. An alternative approach used in some studies is to use a slip condition in a small neighborhood of the contact line to ensure that it moves (see Kamal, Goyal and Chu (1988) and references therein). The slip velocity of the contact line is assumed to be proportional to the shear stress on the wall. This approach however does not ensure that the contact angle remains constant. Another aspect of the floating particle problem

not treated here is that the contact angle for advancing and receding contact lines is different which can change the dynamical behavior of floating particles.

2.3 Reinitialization of ϕ

The level set function ϕ is reinitialized to be a distance function after each time step by solving the following equation obtained in Sussman, et al. (1994) to the steady state

$$\frac{\partial \phi}{\partial t} + \mathbf{w}.\nabla\phi = S(\phi_0) \tag{14}$$

where ϕ_0 is the distribution to be reinitialized and

$$\mathbf{w} = S(\phi_0)\frac{\nabla\phi}{|\nabla\phi|}.$$

Here $S(\phi_0)$ is the sign function, i.e., $S(\phi_0) = 1$ if $\phi_0 > 0$ and $S(\phi_0) = -1$ if $\phi_0 < 0$. In order to avoid discontinuities, in our code we use the following smoothed sign function

$$S(\phi_0) = \frac{\phi_0}{\sqrt{\phi_0^2 + h^2}},$$

where h is equal to one and half times the element size. Equation (14) is a first order hyperbolic partial differential equation which is solved using a positive only upwinding scheme described in Singh and Leal (1993). Clearly, the characteristics of (14) point in the direction of **w**. Therefore, for the points inside the upper fluid **w** points upwards away from the interface and for the points inside the lower fluid it points downwards. Thus, (14) can be solved by specifying the boundary condition $\phi = \phi_0$ at the two-fluid interface $\phi = 0$.

2.4 Variation of fluid properties across the interface

In our finite element scheme the fluid viscosity is assumed to take a jump across the interface, i.e.,

$$\eta = \begin{cases} \eta_l & \text{if } \phi < 0 \\ 0.5(\eta_l + \eta_u) & \text{if } \phi = 0 \\ \eta_u & \text{if } \phi > 0. \end{cases} \tag{15}$$

Here η_l and η_u are the viscosities of the lower and upper fluids, respectively. In other words, the nodes that are above the interface have the upper fluid viscosity and the nodes that are below the interface have

$$\begin{cases}$$

the lower fluid viscosity. The fluid density, on the other hand, is assumed to vary smoothly across the interface

$$\rho = \begin{cases} \rho_l & \text{if } \phi < -h \\ \rho_u & \text{if } \phi > h \\ 0.5(\rho_l + \rho_u) + 0.5(\rho_l - \rho_u)\ \sin\left(\dfrac{\pi\phi}{2h}\right) & \text{otherwise} \end{cases} \tag{16}$$

where h is equal to one and half times the element size, and ρ_l and ρ_u are the densities of the two fluids, respectively. This smoothing of the density is similar to that in Sussman, et al. (1994), and is needed for avoiding numerical instabilities for relatively large density ratio ρ_l/ρ_u.

The surface tension force is smoothed and acts only on the elements for which ϕ is smaller than h. This is done by approximating $\delta(\phi)$ in (6) by a mollified delta function $\delta_h(\phi)$ using the approach described in Sussman, et al. (1994):

$$\delta_h(\phi) = \begin{cases} \dfrac{(1+\cos(\pi\phi/h))}{2h} & \text{for } |\phi| < h \\ 0 & \text{otherwise} \end{cases} \tag{17}$$

The error introduced by smoothing of the surface tension force is O(h). Also note that equations (16) and (17) require that ϕ be maintained as a distance function which we do in our implementation by reinitializing ϕ after each time step.

2.5 Weak form of equations and finite-element discretization

The approach used for obtaining the weak form of the governing equations stated in the previous section was described in Glowinski, et al. (1999) and Singh, et al. (2000). In obtaining this weak form, the hydrodynamic forces and torques acting on the particles can be completely eliminated by combining the fluid and particle equations of motion into a single weak equation of motion for the combined fluid-particle system. The hydrodynamic stresses acting at the interface are also completely eliminated. For simplicity, in this section we will assume that there is only one particle. The extension to the many-particle case is straightforward.

The solution and variation are required to satisfy the strong form of the constraint of rigid body motion throughout P(t). In the distributed Lagrange multiplier method this constraint is removed from the velocity space and enforced weakly as a side constraint using a distributed Lagrange multiplier term. It

was shown in Glowinski, et al. (1999) that the following weak formulation of the problem holds in the extended domain:

For a.e. t>0, find $\mathbf{u} \in \overline{W}_{u\Gamma}$, $p \in L^2_0(\Omega)$, $\boldsymbol{\lambda} \in \Lambda(t)$, $\mathbf{U} \in \mathbf{R}^3$, $\boldsymbol{\omega} \in \mathbf{R}^3$ and $\phi \in W_\phi$, satisfying

$$\int_\Omega \rho_L \left(\frac{d\mathbf{u}}{dt} - \mathbf{g} \right) \cdot \mathbf{v} d\mathbf{x} - \int_\Omega p \nabla . \mathbf{v} \, d\mathbf{x} + \int_\Omega 2\eta \mathbf{D}[\mathbf{u}] : \mathbf{D}[\mathbf{v}] d\mathbf{x}$$
$$+ \left(1 - \frac{\rho_L}{\rho_d} \right) \left(M \left(\frac{d\mathbf{U}}{dt} - \mathbf{g} \right) \cdot \mathbf{V} + I \frac{d\boldsymbol{\omega}}{dt} \boldsymbol{\xi} \right) - \mathbf{F}' . \mathbf{V} - \int_\Omega \gamma \kappa \delta(\phi) \mathbf{n} \cdot \mathbf{v} \, d\mathbf{x} = \left\langle \boldsymbol{\lambda}, \mathbf{v} - (\mathbf{V} + \boldsymbol{\xi} \times \mathbf{r}) \right\rangle_{P(t)}$$

for all $\mathbf{v} \in \overline{W}_0$, $\mathbf{V} \in \mathbf{R}^3$, and $\boldsymbol{\xi} \in \mathbf{R}^3$, (18)

$$\int_\Omega q \nabla . \mathbf{u} \, d\mathbf{x} = 0 \qquad \text{for all } q \in L^2(\Omega), \tag{19}$$

$$\left\langle \boldsymbol{\mu}, \mathbf{u} - (\mathbf{U} + \omega \times \mathbf{r}) \right\rangle_{P(t)} = 0 \qquad \text{for all } \boldsymbol{\mu} \in \Lambda(t), \tag{20}$$

$$\mathbf{u}|_{t=0} = \mathbf{u}_o \qquad \text{in } \Omega, \tag{21}$$

$$\int_\Omega \left(\frac{\partial \phi}{\partial t} + \mathbf{u} \, . \nabla \phi \right) g \, d\mathbf{x} = 0 \quad \text{for all } g \in W_{\phi 0}, \tag{22}$$

$$\phi|_{t=0} = \phi_0 \qquad \text{in } \Omega.$$

as well as the kinematic equations and the initial conditions for the particle linear and angular velocities. Here **F**' is the additional body force applied to the particles to limit the extent of overlap (see equation (19) in Glowinski, et al. (1999)), $\boldsymbol{\lambda}$ is the distributed Lagrange multiplier,

$$\overline{W}_{u\Gamma} = \{ \mathbf{v} \in H^1(\Omega)^3 \mid \mathbf{v} = \mathbf{u}_\Gamma(t) \quad \text{on} \quad \Gamma \},$$
$$\overline{W}_0 = H^1_0(\Omega)^3,$$
$$L^2_0(\Omega) = \{ q \in L^2(\Omega) \mid \int_\Omega q \, d\mathbf{x} = 0 \},$$
$$W_\phi = \{ \phi \in H^1(\Omega) \mid \phi = \phi_0(t) \quad \text{on} \quad \Gamma^- \},$$
$$W_{\phi 0} = \{ \phi \in H^1(\Omega) \mid \phi = 0 \quad \text{on} \quad \Gamma^- \},$$
$$L^2_0(\Omega) = \{ q \in L^2(\Omega) \mid \int_\Omega q \, d\mathbf{x} = 0 \}, \tag{23}$$

where Γ^- is the upstream part of Γ and $\Lambda(t)$ is $L^2(P(t))^3$, with $\langle .,. \rangle_{P(t)}$ denoting the L^2 inner product over the particle. In our simulations, since the velocity and $\boldsymbol{\mu}$ are in L^2, we will use the following inner product

$$\left\langle \boldsymbol{\mu}, \mathbf{v} \right\rangle_{P(t)} = \int_{P(t)} (\boldsymbol{\mu} . \mathbf{v}) \, d\mathbf{x} . \tag{24}$$

In order to solve the above problem numerically, we will discretize the domain using a regular tetrahedral mesh T_h for the velocity, where h is the mesh size, and a regular tetrahedral mesh T_{2h} for the pressure. The following finite dimensional spaces are defined for approximating $\overline{W}_{u\Gamma}$, $\overline{W}_0$, $L^2(\Omega)$, $L_0^2(\Omega)$, W_ϕ and $W_{\phi 0}$:

$$W_{u\Gamma,h} = \{\mathbf{v}_h \in C^0(\overline{\Omega})^3 \mid \mathbf{v}_h|_T \in P_1 \times P_1 \times P_1 \text{ for all } T \in T_h,\ \mathbf{v}_h = \mathbf{u}_{\Gamma,h} \text{ on } \Gamma\},$$

$$W_{0,h} = \{\mathbf{v}_h \in C^0(\overline{\Omega})^3 \mid \mathbf{v}_h|_T \in P_1 \times P_1 \times P_1 \text{ for all } T \in T_h,\ \mathbf{v}_h = 0 \text{ on } \Gamma\},$$

$$L_h^2 = \{q_h \in C^0(\overline{\Omega}) \mid q_h|_T \in P_1 \text{ for all } T \in T_{2h}\},$$

$$L_{0,h}^2 = \{q_h \in L_h^2 \mid \int_\Omega q_h \, d\mathbf{x} = 0\},$$

$$W_{\phi,h}^n = \{g_h \in H^1(\Omega) \mid g_h|_T \in P_1 \text{ for all } T \in T_h,\ g_h = \phi^n \text{ on } \Gamma^-\}$$

$$W_{\phi 0,h} = \{g_h \in H^1(\Omega) \mid g_h|_T \in P_1 \text{ for all } T \in T_h,\ g_h = 0 \text{ on } \Gamma^-\}$$

$$W_{\phi R,h} = \{g_h \in H^1(\Omega) \mid g_h|_T \in P_1 \text{ for all } T \in T_h,\ g_h = 0 \text{ on the interface}\}. \qquad (25)$$

The particle inner product terms in (18) and (20) are obtained using the discrete L^2 inner product defined in Glowinski, et al. (1999). Specifically, we choose M points, $\mathbf{x}_1,\ldots,\mathbf{x}_M$ that uniformly cover $\overline{P}(t)$, and define

$$\Lambda_h(t) = \left\{ \boldsymbol{\mu}_h \;\middle|\; \boldsymbol{\mu} = \sum_{i=1}^{M} \boldsymbol{\mu}_{h,i}\, \delta(\mathbf{x} - \mathbf{x}_i), \quad \boldsymbol{\mu}_{h,1},\ldots,\boldsymbol{\mu}_{h,M} \in \mathbf{R}^3 \right\}.$$

Using these finite dimensional spaces, it is straightforward to discretize equations (18) - (22). Notice that the discrete space $W_{\phi,h}$ assumes that ϕ is known on the upstream portion of the boundary. This is not a problem even when $\phi(t)$ is not known on the upstream boundary in advance because the imposed boundary value can be corrected during the reinitialization step. Also notice that since only the zero level set of $\phi(t)$ is physically relevant, we have a lot of freedom in treating $\phi(t)$ away from the interface. In our code, the value from the previous time step is used as the boundary value. Also note that the reinitialization space $W_{\phi R,h}$ assumes that ϕ remains zero along the interface which is done by imposing Dirichlet boundary condition, $\phi = 0$, along the interface during reinitialization iterations.

2.6 Strong form

The strong form for the weak formulation can be obtained by integrating the stress term by parts. The resulting equations inside the region occupied by the fluid $\Omega\backslash\overline{P(t)}$ are

$$\rho_L\left[\frac{\partial \mathbf{u}}{\partial t}+\mathbf{u}.\nabla\mathbf{u}\right] = \rho_L\mathbf{g} - \nabla p + \nabla.\boldsymbol{\sigma} + \gamma\,\kappa\,\delta(\phi)\,\mathbf{n} \qquad \text{in } \Omega\backslash\overline{P(t)}$$

$$\nabla\cdot\mathbf{u} = 0 \qquad \text{in } \Omega\backslash\overline{P(t)}$$

$$\mathbf{u} = \mathbf{u}_L \qquad \text{on } \Gamma$$

$$\mathbf{u} = \mathbf{U} + \omega \times \mathbf{r} \qquad \text{on } \partial P(t)$$

and the equations inside the region occupied by the particles P(t) are

$$\rho_L\left[\frac{\partial \mathbf{u}}{\partial t}+\mathbf{u}.\nabla\mathbf{u}\right] = \rho_L\mathbf{g} - \nabla p + \nabla.(2\eta\mathbf{D}) + \boldsymbol{\lambda} - R^2\nabla^2\boldsymbol{\lambda}$$

$$\mathbf{u} = \mathbf{U}_i + \omega_i \times \mathbf{r}_i \qquad \text{on } \partial P_i(t)\,,\ i=1,\ldots,N,$$

Here we have used the fact that the rigid body motion satisfies the incompressibility constraint and that $\mathbf{D(u)}$ inside the particles is zero. The boundary condition for $\boldsymbol{\lambda}$ on the interface between the fluid and particle regions $\partial P(t)$ is

$$\mathbf{n}.(-\sigma_L) = \mathbf{n}.\nabla\boldsymbol{\lambda}$$

where $\mathbf{n}$ is the normal at the fluid-particle interface, and $\sigma_L = -p\mathbf{I} + 2\eta\mathbf{D}$ is the stress in the fluid phase, and $\sigma_P = 0$ is the stress inside the particles. For given $\mathbf{U}(t)$ and $\omega(t)$, and the positions $X_i(t)$, i=1,…, N, equation (26) can be written as:

$$\boldsymbol{\lambda} - R^2\nabla^2\boldsymbol{\lambda} = \rho_L\left(\frac{d\mathbf{U}}{dt}+\frac{d\omega}{dt}\times\mathbf{r} + \omega\times(\omega\times\mathbf{r}) - \mathbf{g}\right)$$

2.7 Time discretization using the Marchuk-Yanenko operator splitting scheme

The discretized initial value problem (18-22) is solved by using the Marchuk-Yanenko operator splitting scheme. This allows us to decouple its four primary difficulties:

1. The incompressibility condition and the related unknown pressure p_h,
2. The nonlinear convection term,
3. The rigid body motion problem inside the particles,
4. The interface problem and the related unknown level set distribution ϕ_h,

The Marchuk-Yanenko operator splitting scheme can be applied to an initial value problem of the form

$$\frac{d\phi}{dt} + A_1(\phi) + A_2(\phi) + A_3(\phi) + A_4(\phi) = f$$

where the operators A_1, A_2, A_3, and A_4 can be multiple-valued.

Let Δt be the time step, and α_1 and α_2 be two constants: $0 \le \alpha_1, \alpha_2 \le 1$ and $\alpha_1 + \alpha_2 = 1$. We use the following version of the Marchuk-Yanenko operator splitting to simulate the motion of particles on two-fluid interfaces:

Set $\mathbf{u}^0 = \mathbf{u}_{0,h}$, and $\phi^0 = \phi_{0,h}$.

For n = 0,1,2,… assuming $\mathbf{u}^n$, and ϕ^n are known, find the values for n+1 using the following:

STEP 1:

Find $\mathbf{u}^{n+1/4} \in W_{u,h}$ and $p^{n+1/4} \in L^2_{0,h}$, by solving

$$\int_\Omega \rho_L \frac{\mathbf{u}^{n+1/4} - \mathbf{u}^n}{\Delta t} \cdot \mathbf{v}\, d\mathbf{x} - \int_\Omega p^{n+1/4} \nabla \cdot \mathbf{v}\, d\mathbf{x} = \int_\Omega \gamma \kappa \delta(\phi) \mathbf{n} \cdot \mathbf{v}\, d\mathbf{x}$$

$$\text{for all } \mathbf{v} \in W_{0,h},$$

$$\int_\Omega q \nabla \cdot \mathbf{u}^{n+1/4}\, d\mathbf{x} = 0 \qquad \text{for all } q \in L^2_h, \tag{26}$$

STEP 2:

Find $\mathbf{u}^{n+2/4} \in W_{u,h}$, by solving

$$\int_\Omega \rho_L \frac{\mathbf{u}^{n+2/4} - \mathbf{u}^{n+1/4}}{\Delta t} \cdot \mathbf{v} d\mathbf{x} + \int_\Omega \rho_L (\mathbf{u}^{n+2/4} \cdot \nabla \mathbf{u}^{n+2/4}) \cdot \mathbf{v}\, d\mathbf{x} + \alpha_1 \int_\Omega 2\eta \mathbf{D}[\mathbf{u}^{n+2/4}] : \mathbf{D}[\mathbf{v}] d\mathbf{x} = 0$$

$$\text{for all } \mathbf{v} \in W_{0,h}, \tag{27}$$

STEP 3:

Compute $\mathbf{U}^{n+3/4}$ and $\mathbf{X}^{n+3/4}$ using the prediction procedure

Set $\mathbf{U}^{n,0} = \mathbf{U}^n$, $\mathbf{X}^{n,0} = \mathbf{X}^n$.

Do k=1,K

$$\mathbf{U}^{*n,k} = \mathbf{U}^{n,k-1} + \left(\mathbf{g} + \left(1 - \frac{\rho_L}{\rho_d} \right)^{-1} M^{-1} F'(X^{n,k-1}) \right) \frac{\Delta t}{K}$$

$$\mathbf{X}^{*n,k} = \mathbf{X}^{n,k-1} + \left(\frac{\mathbf{U}^{n,k-1} + \mathbf{U}^{*n,k}}{2} \right) \frac{\Delta t}{K}$$

$$\mathbf{U}^{n,k} = \mathbf{U}^{n,k-1} + \left(\mathbf{g} + \left(1 - \frac{\rho_L}{\rho_d} \right)^{-1} M^{-1} \frac{F'(X^{n,k-1}) + F'(X^{*n,k-1})}{2} \right) \frac{\Delta t}{K}$$

$$\mathbf{X}^{n,k} = \mathbf{X}^{n,k-1} + \left(\frac{\mathbf{U}^{n,k-1} + \mathbf{U}^{n,k}}{2} \right) \frac{\Delta t}{K}$$

end do

Set $\mathbf{U}^{n+3/4} = \mathbf{U}^{n,K}$, $\mathbf{X}^{n+3/4} = \mathbf{X}^{n,K}$. (28)

Find $\mathbf{u}^{n+1} \in W^{n+1}_{u\Gamma,h}$, $\boldsymbol{\lambda}^{n+1} \in \Lambda_h((n+2/4)\Delta t)$, $\mathbf{U}^{n+1} \in \mathbf{R}^3$, and $\boldsymbol{\omega}^{n+1} \in \mathbf{R}^3$, satisfying

$$\int_\Omega \rho_L \frac{\mathbf{u}^{n+1} - \mathbf{u}^{n+2/4}}{\Delta t} . \mathbf{v}\, d\mathbf{x} + \left(1 - \frac{\rho_L}{\rho_d} \right) \left(M \frac{\mathbf{U}^{n+1} - \mathbf{U}^{n+3/4}}{\Delta t} . \mathbf{V} + I \frac{\boldsymbol{\omega}^{n+1} - \boldsymbol{\omega}^{n+3/4}}{\Delta t} \boldsymbol{\xi} \right) +$$

$$\gamma \int_\Omega 2\eta \mathbf{D}[\mathbf{u}^{n+1}] : \mathbf{D}[\mathbf{v}] d\mathbf{x} = \left\langle \boldsymbol{\lambda}^{n+1}, \mathbf{v} - (\mathbf{V} + \boldsymbol{\xi} \times \mathbf{r}^{n+3/4}) \right\rangle_{P((n+3/4)\Delta t)}$$

for all $\mathbf{v} \in W_{0,h}$, $\mathbf{V} \in \mathbf{R}^3$, and $\boldsymbol{\xi} \in \mathbf{R}^3$

$$\left\langle \boldsymbol{\mu}_h, \mathbf{u}^{n+1} - (\mathbf{U}^{n+1} + \boldsymbol{\omega}^{n+1} \times \mathbf{r}) \right\rangle_{P((n+3/4)\Delta t)} = 0 \qquad \text{for all } \boldsymbol{\mu}_h \in \boldsymbol{\Lambda}((n+3/4)\Delta t), \tag{29}$$

where the center of particle $P((n+3/4)\Delta t)$ is at $X^{n+3/4}$.

Set $\mathbf{X}^{n+1,0} = \mathbf{X}^n$.

Do k=1,K

$$\mathbf{X}^{*n+1,k} = \mathbf{X}^{n+1,k-1} + \left(\frac{\mathbf{U}^n + \mathbf{U}^{n+1}}{2} \right) \frac{\Delta t}{K}$$

$$\mathbf{X}^{n,k} = \mathbf{X}^{*n,k-1} + \left(1 - \frac{\rho_L}{\rho_d} \right)^{-1} M^{-1} \left(\frac{F'(X^{n+1,k-1}) + F'(X^{*n+1,k})}{2} \right) \frac{(\Delta t)^2}{2K}$$

end do

Set $\mathbf{X}^{n+1} = \mathbf{X}^{n+1,K}$.

STEP 4:

Find $\phi^{n+4/4} \in W^n_{\phi,h}$, by solving

$$\int_{\Omega}\left(\frac{\phi^{n+4/4}-\phi^{n}}{\Delta t}+\mathbf{u}^{n+1}.\nabla\phi^{n+1}\right)g_h d\mathbf{x} \quad = \quad 0$$

for all $g_h \in W_{\phi 0,h}$. (30)

Set $p^{n+1}= p^{n+1/4}$, $\phi^{n+1} = \phi^{n+4/4}$.

STEP 4.1:

Reinitialize ϕ^{n+1}

Set $\phi_R^0 =\phi^{n+1}$

For r = 0, 1, 2, …

$$\mathbf{w}^r = S(\phi^{n+1})\frac{\nabla\phi_R^r}{\left|\nabla\phi_R^r\right|}$$

Find $\phi_R^{r+1} \in W_{\phi R,h}$, by solving

$$\int_{\Omega}\left(\frac{\phi_R^{r+1}-\phi_R^r}{\Delta t}+\mathbf{w}^r.\nabla\phi_R^r\right)g_h d\mathbf{x} \quad = \int_{\Omega} S(\phi^{n+1})\, g_h \, d\mathbf{x}$$

for all $g_h \in W_{\phi R,h}$. (31)

go back to the above for loop.

STEP 4.2:

Modify ϕ^{n+1} inside and on the particle surfaces to enforce contact angle

$$\frac{\partial\phi}{\partial t}+\mathbf{u}_{ex}.\nabla\phi = 0$$

Set $\phi_R^0 =\phi^{n+1}$

For r = 0, 1, 2, …

$$\mathbf{u}_{ex}^r = \begin{cases} 0 & \text{outside particles} \\ \mathbf{u}_{ex} \text{ from (12)} & \text{otherwise} \end{cases}$$

Find $\phi_R^{r+1} \in W_{\phi R,h}$, by solving

$$\int_{\Omega}\left(\frac{\phi_R^{r+1}-\phi_R^{r}}{\Delta t}+\mathbf{u_{ex}}^{r}.\nabla\phi_R^{r}\right)g_h\,d\mathbf{x}\quad=0$$

$$\text{for all } g_h \in W_{\phi R,h}. \tag{32}$$

go back to the above for loop.

Set $\phi^{n+1} = \phi_R^{r+1}$ and go back to the first step.

The decoupled sub-problems can be solved much more efficiently than the original problem (18-22). In our code all of these sub-problems are solved using matrix-free algorithms, which reduces the memory required.

Remarks:

1. The first step gives rise to a L^2 projection problem for the velocity and pressure distributions which is solved by using a conjugate gradient method (Glowinski, Tallec, Ravachol and Tsikkinis (1992) and Glowinski, et al. (1999)).

2. The second step is a nonlinear problem for the velocity, which is solved by using a least square conjugate gradient algorithm (Glowinski and Pironneau (1992)).

3. In this paper, we will assume that $\alpha_1 = 1$, $\alpha_2 = 0$.

4. The fourth step is a hyperbolic problem for the scalar level set function ϕ. This problem is solved by using a upwinding scheme where the advection term is discretized using a third order scheme (Glowinski and Pironneau (1992) and Pillaipakkam and Singh (2001)).

5. After advecting ϕ according to (30), we reinitialize ϕ to be a distance function near the interface by performing one or two iterations of (31) using a fast algorithm developed in Pillaipakkam and Singh (2001). The interface position $\phi(t) = 0$ does not change during these reinitialization iterations. It is necessary to re-initialize ϕ to ensure that the scheme accurately conserves mass.

6. The level set function is extended inside and on the surface of the particles such that the contact angle is 135 degrees by performing one or two iterations of (32).

3. Results

In this section we discuss the numerical results obtained using the above algorithm for the motion of spherical particles trapped on two-fluid interfaces. The domains used in our simulations are box shaped with rectangular cross sections. Simulations are started by assuming that the higher density fluid is at the bottom and the lower density fluid is at the top and the interface between the two fluids is flat. The

coordinate system used throughout this paper is shown in figure 7. The x-, y- and z-components of particle velocity will be denoted by u, v and w, respectively.

We will also assume that all dimensional quantities, unless otherwise noted, are in the CGS units. The lower fluid density ρ_L=1.0 gm/cm^3 and viscosity is 1.0 Poise. The density and viscosity of the upper fluid are varied and the particle density is assumed to be greater than one. The particle diameter is assumed to be 0.2 cm. The interfacial tension value is selected to ensure that the particle remains suspended along the interface. The dynamic contact angle is assumed to be equal to the static contact angle which is assumed to be 135 degrees. The acceleration due to gravity g=981.0 gm/cm^2 and acts along the negative z-direction. The initial fluid velocity is assumed to be zero everywhere. The initial particle velocities are also assumed to be zero.

No slip boundary condition is applied on the surface of the box shaped computational domains. The contact angle between the interface and the box boundaries is assumed to be 90 degrees which ensures that the interface near walls is flat and, as noted above, the contact angle between the interface and the particle is assumed to be 135 degrees.

We next present the results of several simulations, to demonstrate that the scheme works correctly, and that it reproduces the expected dynamical behavior and the static equilibrium state.

3.1. Motion of a single particle

In this subsection we investigate the case where a single spherical particle is released along the interface, i.e., the contact line intersects the particle surface[1], at a position which is different from that for static equilibrium. The initial interface shape is assumed to be flat, except near the particle surface where a contact angle of 135 degrees is prescribed (see figure 6). The parameters are the range for which a particle trapped on the interface can be in static equilibrium. The equilibrium interface shape and the particle floating height depend on the problem parameters.

As discussed in section 1, a particle trapped on a two-fluid interface can be in a state of static equilibrium, even when it is heavier than both liquids, provided its buoyant weight is balanced by the vertical component of capillary force. Also, in equilibrium, the interface shape must be such that the interfacial tension is exactly balanced by a jump in the pressure across the interface and therefore no fluid flow is induced. However, when a particle is suddenly released along the interface, the interface shape evolves to the equilibrium shape in a finite time interval. During this time interval, the velocity field in the

[1] If the initial particle position was such that the contact line did not intersect the particle surface, then we would also need to address the problem of an interface coming in contact with a solid surface. This would require us to include additional physics to specify the conditions under which an interface can touch a solid surface. This physics is not included in the current version of our code.

two fluids is non-zero and the interfacial force acting on the particle varies. As a result, the particle velocity and its vertical position relative to the interface change with time. The final static state, as described by analytical expressions (1-3), however, is independent of these transients and can be used to verify the accuracy of numerical results.

We first present results that show that the trajectory of a particle released along the two-fluid interface is independent of the mesh resolution and the time step. We have used two regular tetrahedral meshes to show that the results converge with mesh refinement. In a tetrahedral element there are seven velocity and four pressure nodes. The rigid body constraint inside particles is enforced using uniformly distributed collocation points. The number of velocity nodes and elements in the first mesh are 117,649 and 13,824, respectively. In the second mesh, referred to as mesh B, there are 249,985 velocity nodes and 124,416 elements. The time step for these simulations is 0.0001, 0.00005 or 0.000025.

The particle density is 1.05 gm/cm^3 and the interfacial tension is 16.0 dynes/cm. For the upper fluid density is 0.1 gm/cm^3 and the viscosity is 0.1 Poise. The initial velocity distribution in the fluid, and the particle's linear and angular velocities are assumed to be zero. The domain is assumed to cubical with sides 0.4 cm. The particle center is at a distance of h=0.02 cm above the undeformed interface which passes though the domain center.

From figure 8, where w is plotted as a function of time for three different values of time step and two different mesh resolutions, we note that when the time step is reduced or when the mesh is refined the variation of w with time remains approximately the same. This allows us to conclude that the numerical results converge with both mesh and time step refinements.

From figures 8 we notice that the vertical component of particle velocity w increases for t<~0.005 s and then it starts to decrease. It becomes negative for t=~0.019 s and then increases again and becomes very small and fluctuates around zero for t>~0.06 s. The other components of velocity u and v remain small for all times. We will assume that for t=0.06 s the particle has reached a state of static equilibrium with h_2=0.156R and θ_c=65.26 . These values are in good agreement with the static equilibrium requirements (1-3), as discussed in table 1. We may therefore conclude that the state of static equilibrium is captured correctly by our code.

In order to understand the reason for the initial increase in w, we notice that the angle θ_c, i.e., the position of the contact line on the particle surface, in figure 7a is larger than that for the equilibrium state shown in figure 7b (also see figure 6). Thus, from figure 3 it is clear that the vertical component of interfacial force is initially larger and as a result the particle moves upwards. This is a consequence of the fact that initially the interface is approximately flat everywhere except near the particle surface (see figure 7a). But, with increasing time, due to the interfacial tension the fluid level around the particle decreases and the interface takes its characteristic parabolic shape. Thus, the contact line position on the particle

surface moves downwards and the vertical component of interfacial force decreases. Also notice that the vertical component of the pressure force in figures 7a and b are different, but in figure 7a the fluid velocity is not small and so the pressure force cannot be determined using hydrostatics.

To verify our code further, we performed calculations for five different values of interfacial tension γ while keeping the other parameters fixed. Figure 9 shows that, as expected, when γ is smaller the particle sinks to a greater depth. In table 1 we have listed the floating heights and the sum of the pressure and vertical component of interfacial forces acting on the particle for these five values of the interfacial tension. For all cases in equilibrium, as required, $F_p + F_c$ is approximately equal to the particle's weight. There are small differences due to numerical errors.

In table 2 we have listed the floating heights for two additional cases where the density of the upper fluid is 0.01 gm/cm^3 and 0.0016 gm/cm^3 and the corresponding viscosities are 0.033 Poise and 0.0166 Poise. The interfacial tension is 16.0 dynes/cm. The step used for these calculations was $2\text{x}10^{-5}$. The domain was discretized using mesh B described above. The other parameters are the same as above. The table shows that as expected the floating height decreases slightly when the density of the upper is reduced as for the case considered above it is already a fraction of that for the lower fluid. The time step required, however, is smaller and decreases as the ratio of lower and upper density increases. The same is true when the viscosity ratio is large.

The static equilibrium analysis, presented in section 1, assumes that the fluid extends to infinity in the x-, y- and z-directions which is not the case for our simulations. This may also explain some difference between our simulations and the analytical results. These differences are expected to decrease with increasing box size. We also wish to note that for our simulations the magnitude of fluid velocity decreases as the state of equilibrium is approached, but it does not decrease beyond a value that depends on the fluid viscosity, surface tension and the interface curvature. The flow develops steady spurious circulation cells around the interface that are similar those seen in simulations of drops (Scardovelli and Zaleski (1999)). It has been noted by D.D. Joseph that these circulation cells arise in simulations because the discretized equation for the vorticity, which can be obtained by taking the curl of the momentum equation, contains a non zero contribution from the surface tension term. This creates vorticity along the discretized interface which diffuses into the domain. The presence of these cells, however, does not seem to affect the overall force balance, discussed in table 1, for static equilibrium.

3.2. Motion of two particles

We next present results for the case where two spherical particles are released near each other along the interface at the same vertical height. The initial interface position is assumed to be flat, except near the particle surfaces where a contact angle of 135 degrees is prescribed. The initial vertical height of

the particles is different from that for the static equilibrium of a single particle. The parameters are assumed to be in the range for which the particles trapped on the interface can be in static equilibrium.

For these calculations the particle density is 1.05 gm/cm^3. The interfacial tension is 16.0 dynes/cm. The upper fluid density is 0.01 gm/cm^3 and the viscosity is 0.033 Poise. The initial velocity distribution in the fluid and the particle velocities are assumed to be zero. The domain height is 0.5 cm. The width along the x-direction is 0.5 cm and along the y-direction is 1.0 cm. The undeformed interface passes though the domain center and initially the particle centers are at a height of h=0.02 cm above the interface. The initial distance between the particles in the y-direction is 1.2 R. The mesh resolution is comparable to that for the coarse mesh in section 3.1. The number of velocity nodes and elements are 141,285 and 16,184 respectively.

We have already noted that when two or more particles released along the interface are close they move towards each other due to the action of the lateral component of interfacial tension which arises due the asymmetric deformation of the interface around the particles. Figure 10a shows that for t=0.02 the interface shape is deformed in a small region around the particles and away from the particles it is relatively flat and there is no lowering of interface between the particles. Hence, at this time, the particles do not experience any lateral attractive force. But, as was the case for a single particle, the interface height around the particles decreases as t increases and, as a result, the contact lines for both particles move downward. The vertical component of interfacial force which is initially larger than the steady state value causes the particles to move upward, but as the contact lines move downward the vertical interfacial force decreases and the vertical particle velocities become negative. After, this initial motion for t<~0.05 s, the vertical particle velocities become relatively small, but, as discussed below, remain negative as the particles approach each other. These initial transients in the vertical component of particle velocities could be diminished by setting their initial positions and interface shape close to that for the equilibrium of an isolated particle. This would however complicate the problem of prescribing initial conditions and make the problem less realistic.

In figure 10b the particle positions and the interface shape are shown at t=0.59. Due to the lowering of the contact lines on the particle surfaces the interface height between the particles is also lowered. This leads to further lowering of the contact lines between the particles. Consequently, the interface shape and the contact lines for the particles are no longer symmetric about the vertical through their respective centers. Thus, the lateral component of interfacial force acting on the particles is not zero which causes them to move toward each other. As the particles move toward each other, the interface shape evolves throughout the domain. The time taken for the lowering of the contact lines between the particles depends on the distance between the particles which in this case is relatively short as the particles are relatively close to each other.

The particle positions and interface shape at t=0.82 are shown in figure 10c; The interface height and the contact line positions between the particles are significantly lower than on the sides. Thus, the magnitude of the attracting interfacial force in figure 10c is larger than for figure 10a. This is also seen as an increase in the approach velocity v_2-v_1 in the lateral component of particle velocities plotted as a function of time in figure 11. The simulations were stopped at t=1.05 when the distance between the particles reduced to 0.012. The interface shape at this time is shown in figure 10d. Notice that the interface height between the particles in this figure is even lower and the interface shape is flatter.

Another interesting consequence of the lowering of interface height and contact lines between the particles, as they approach each other, is that there is a decrease in the vertical component of interfacial force acting on the particles. The vertical component of interfacial tension acts against gravity and keeps them floating on the interface even though they are heavier than both liquids. This decrease in the vertical interfacial force causes the floating height of the particles to decrease slightly (see table 3). For example, the height for a single particle in section 3.1 for the same parameters was 0.419, but for the two particles in figure 10d it is 0.375, where they are almost touching. This decrease in the floating height raises the contact line position everywhere on the particles and the vertical component of interfacial force increases back to the value required for balancing the buoyant weight. It is worth noting that when the parameters are such that for an isolated particle the sum of the vertical component of the interfacial and pressure forces is near its maximum value, a decrease in the floating height would actually decrease the vertical component of total force. Therefore, if the particles are barely floating a decrease in the floating height will lead to the sinking of both particles. This suggests that the clusters of particles are more likely to sink than an isolated particle.

3.3. Motion of four particles

Finally, we consider the case where four spherical particles are released near each other along the interface at the same vertical height. The initial interface position is assumed to be flat, except near the particle surfaces where the contact angle is assumed to be 135.

For these calculations the particle density is 1.05 gm/cm^3 and the interfacial tension is 16.0 dynes/cm. The upper fluid density is 0.1 gm/cm^3 and the viscosity is 0.1 Poise. The motion starts from rest. The domain height is 0.4 cm. The width along x-direction is 0.8 cm and along y-direction is 0.8 cm. The undeformed interface passes though the domain center. The initial positions of the four particles are (0.4,0.22,0.22), (0.4,0.58,0.22), (0.23,0.4,0.22) and (0.57,0.4,0.22). The mesh resolution is the same as for the coarse mesh in section 3.1.

In this case, as for the single and two-particle problems, after initial variations in the vertical components of particle velocities, the particles begin to move toward each other. Their vertical velocity

becomes small at t=0.05 and around this time the interface height between the particles begins to decrease.

In figures 12a and b the particle and interface shape are shown at t=0.02 and 0.96, respectively. In the first figure the interface shape between particles is not significantly deformed and the lateral velocities are small and in the second figure the interface height between the particles is already lowered. The interface shape and the contact lines for the particles are no longer symmetric and thus the lateral component of interfacial force acting on the particles is not zero which causes them to move laterally towards each other.

As particles approach each other, the vertical component of interfacial force decreases due to the lowering of interface height between the particles and thus the floating height of the particles decreases slightly (see figure 12b). For example, the height for a single particle in section 3.1 for the same parameters is 0.419, for the two particle case it is 0.375, and for the four particles in figure 12b, where they are almost touching, it is 0.355.

4. Conclusions

This is the first paper on the direct numerical simulation of the motion of solid floating particles. A floating particle, embedded in the interface between two fluids, touches the interface at a fixed contact angle, which at equilibrium given is by Young's law. The problem of the motion of contact line is difficult and unsolved. The problem is that the no slip condition implies that the contact point cannot move which contradicts the behavior seen in experiments (see Dussan and Davis (1974), Dussan (1976) and Kistler and Scriven (1993) and references therein). Several approaches to this problem have been proposed and could be implemented in direct numerical simulations (see Sussman (2001), Friedrichs and Guceri (1993), Kamal, Goyal and Chu (1988), and references therein). Here we look at one approach which could be called capillary induced motion of the contact line due to a prescribed contact angle. In this approach we let the contact line adjust to the dynamics under the constraint that the contact angle is fixed. The no slip condition is satisfied before and after the contact line moves. In another approach, not implemented here, the contact line is allowed to slip by relaxing the no slip condition by putting the velocity of the contact line proportional to the shear stress there. This approach requires us to relax of the prescribed contact angle condition. Another feature, not treated here, which impacts the floating particle problem is the existence of advancing and receding contact angle. The subject is very rich with many possibilities that might be studied in direct simulations.

The Marchuk-Yenenko operator-splitting technique is used to decouple the four primary numerical difficulties of the governing equations: incompressibility constraint, nonlinear convection term, Lagrange multiplier problem that forces rigid body motion within the particles, and the interface

advection problem. The resulting four sub-problems are solved efficiently using matrix free approaches. Specifically, the DLM approach is used for enforcing rigid body motion inside the particles, the level set approach for tracking the interface and the conjugate gradient algorithms are used to enforce the incompressibility constraint and to solve the nonlinear convection problem. The code is validated by simulating the time dependent motion of a particle released on a two-fluid interface to steady state. Our simulations show that the interface shape near a particle adjusts quickly after it is released to meet the contact angle requirement, but away from the particle the interface shape takes a much longer time interval to adjust during which the vertical position of particle changes. The obtained results are shown to be independent of the mesh resolution as well as the size of time step. We also show that the steady state results of our dynamic simulations agree with the static equilibrium results. The time dependent simulations of two or more floating particles show that they attract each other and form clusters. The attractive capillary force arises due to the asymmetric interface deformation around the particles. Specifically, the interface height between the particles is lowered which gives rise to a lateral attractive force due to gravity and capillarity. This lowering of the interface also decreases the net vertical component of the interfacial force which causes the floating height of the particles to decrease. These results agree qualitatively with the experimental data as well as the static equilibrium analysis.

Acknowledgements

This paper is dedicated to Professor Stan Osher on the occasion of his 60th birthday. This work was partially supported by National Science Foundation KDI Grand Challenge grant (NSF/CTS-98-73236) and a GOALI grant NSF/CTS-0109079, Engineering Research Program of the Office of Basic Energy Science at DOE, a grant from Schlumberger foundation, from STIM-LAB Inc., New Jersey Commission on Science and Technology through the New-Jersey Center for Micro-Flow Control under (Award Number 01-2042-007-25) and the University of Minnesota Supercomputing Institute.

5. References

1. Bowden, N., I.S. Choi, B.A. Grzybowski, G.M. Whitesides, Mesoscale self-assembly of hexagonal plates using lateral capillary forces: synthesis using the "capillary bond", *J. Am. Chem. Soc.* 121, 5373-5391 (1999).
2. Bowden, N., A. Terfort, J. Carbeck, G.M. Whitesides, Self-assembly of mesoscale objects into ordered two-dimensional arrays, Science, 276, 233-235. (1997).
3. Brenner, H. and L.G. Leal. A micromechanical derivation of Fick's law for interfacial diffusion of surfactant molecules, *J. Colloid Interface Sci.* **65**, 191 (1978).
4. Brenner, H. and L.G. Leal. Conservation and constitutive equations for adsorbed species undergoing surface diffusion and convection at a fluid-fluid interface, *J. Colloid Interface Sci.* **88**, 136 (1982).
5. Bristeau, M.O., R. Glowinski & J. Periaux. Numerical methods for Navier-Stokes equations. Application to the simulation of compressible and incompressible flows, *Computer Physics Reports,* **6**, 73 (1987).
6. Chan, D.Y.C., J.D. Henry Jr. and L.R. White. The interaction of colloidal particles collected at the fluid interface, *J. Colloid Interface Sci*. **79**, 410 (1981).
7. Danov, K.D., R. Aust, F. Durst and U. Lange. Influence of the surface viscosity on the hydrodynamic resistance and surface diffusivity of a large Brownian particle, *J. Colloid and Interface Science*, **175**(1), Oct 36-45 (1995).
8. Dussan V., E.B. and S.H. Davis. On the motion of a fluif-fluid interface along a solid surface. *J. Fluid Mech.* **65**, 71 (1974).
9. Dussan V., E.B. The moving contact line: the slip boundary condition. *J. Fluid Mech.* **77**, 665-684 (1976).
10. Fortes, M.A. Attraction and repulsion of floating particles, *Can. J. Chem.* **60,** 2889 (1982).
11. Friedrichs, B. and S.I.Guceri. A novel hybrid numerical technique to model 3-D fountain flow in injection molding processes, *J. Non-Newtonian Fluid Mech.* **49**, 141-173 (1993).
12. Gerson, D.F., Zaijc, J.E. and Ouchi, M.D. Chemistry for energy, Ed. M. Tomlinson, ACS symposium series, 90, American Chemical Society, Washington DC, 1979, pp 66.
13. Gifford, W.A. and L.E. Scriven. On the attraction of floating particles, *Chem. Engrg. Sci.* **26**, 287-297 (1971).
14. Glowinski, R., T.W. Pan, T.I. Hesla & D.D. Joseph. A distributed Lagrange multiplier/fictitious domain method for particulate flows, *Int. J. Multiphase Flows* **25(5)**, 755 (1999).
15. Glowinski, R. and O. Pironneau. Finite element methods for Navier-Stokes equations, *Annu. Rev. Fluid Mech*. **24**, 167 (1992).
16. Glowinski, R., P. Tallec, M. Ravachol & V. Tsikkinis. Chap. 7 in *Finite Elements in Fluids, Vol 8*, Ed. T.J. Chung, Hemisphere Publishing Corp., Washington DC (1992).
17. Goldman, A.J., R.G. Cox and H. Brenner. Slow viscous motion of a sphere parallel to a plane wall—I Motion through a quiescent fluid, *Chem. Eng. Sci*. **22**, 637-653 (1967).
18. Grzybowski, B.A., N. Bowden, F. Arias, H. Yang, G.M. Whitesides, Modeling of menisci and capillary forces from the millimeter to the micrometer size range, *J. Phys. Chem. B* 105, 404-412. (2001).
19. Hirt, C.W. and B.D. Nichols, Volume of fluid (VOF) methods for the dynamics of free boundaries, *J. Comput. Phys.* **39**, 201 (1981).
20. Kamal, M.R., S.K. Goyal and E. Chu. Simulation of injection mold filling of viscoelastic polymer with fountain flow, *AIChE Journal*, **34**, 94-106 (1988).
21. Katoh, K., H. Fujita and E. Imazu. Motion of a particle floating on a liquid meniscus surface, *J. Fluids Engrg.* **114**, 411 (1992).

22. Kistler, S.F. and L.E. Scriven. The teaplot effect: sheet-forming flows with deflection, wetting and hysteresis, *J. Fluid Mech.* **263**, 19-62 (1994).
23. Kralchevsky, P.A., V.N. Paunov, N.D. Denkov, I.B. Ivanov and K. Nagayama. Energetical and force approaches to the capillary interactions between particles attached to a liquid-fluid interface, *J. Colloid and Interface Sci.* **155**, 420-437 (1993).
24. Kralchevsky, P.A., V.N.Paunov, I.B.Ivanov and K.Nagayama, "Capillary Meniscus Interactions between Colloidal Particles Attached to a Liquid - Fluid Interface", *J. Colloid Interface Sci.* 151 (1992) 79 - 94.
25. Kralchevsky, P. A. and K. Nagayama, "Capillary interactions between particles bound to interfaces, liquid films and biomembranes", Advances in Colloid and Interface Science, 85 (2000) 145-192.
26. Manon, V.B. and D.T. Wasan. Particle-fluid interactions with application to solid-stabilized emulsions. Part 1, The effect of asphaltene adsorption. *Colloids Surf.* **19**, 89-105 (1986).
27. Marchuk, G.I. Splitting and alternate direction methods. *Handbook of Numerical Analysis*, P.G. Ciarlet and J.L. Lions (Eds.), Volume I, 197-462. Amsterdam: North-Holland (1990).
28. Nicolson, M.M. The interaction between floating particles, *Proc. Cambridge Philosophical Soc.,* **45**, 288 (1949).
29. Osher, S. and J.A. Sethian. Fronts propagating with curvature-dependent speed: Algorithms based on Hamilton-Jacobi formulations, *J. Comput. Phys.* **83**, 12 (1988).
30. Petkov, J.T., N.D Denkov, K.D Danov, O.D. Velev, R. Aust and F Durst. Measurement of the drag coefficient of spherical particles attached to fluid interfaces, *J. Colloid and Interface Science,* **172**, 147-154 (1995).
31. Pillaipakkam, S.B. and P. Singh. A Level Set Method for computing solutions to viscoelastic two-phase flow, *J. Computational Physics,* **174**, 552-578 (2001).
32. Poynting, J.H. and J.J. Thompson. *A Text-book of Physics: Vol. 1, Properties of Matter*, C. Griffith & Co. Ltd, London, p. 153-155 (1913).
33. Princen, H.M. Equilibrium shape of interfaces, drops and bubbles. Rigid and deformable particles at interfaces, *Surface and Colloid Science*, E. Matijevie, ed., Interscience, New York, Vol. 2, p.1 (1969).
34. Rapacchietta A.V. and A.W. Neumann. Force and free-energy analyses of small particles at fluid interfaces: II. Spheres, *J. Colloid and Interface Sci.*, **59**(3), 555-567 (1977).
35. Redoev, B., M. Nedjalkov and V. Djakovich. Brownian motion at liquid-gas interfaces. I. Diffusion coefficients of maroparticles at pure interfaces, *Langmuir,* **8**, 2962 (1992).
36. Ryskin, G. & L.G. Leal. Numerical solution of free-boundary problems in fluid mechanics. Part 1: The finite-difference technique, *J. Fluid Mech*. **148**, 1 (1984).
37. Scardovelli, R. and Zaleski, S., Direct Simulation of Free-surface and interfacial flow, *Annu. Re. Of Fluid Mech.* 1999 **31**: 567-603.
38. Schneider, Y.C., M.E. O'Neill, and H. Brenner. On the slow viscous rotation of a body straddling the interface between two immiscible semi-infinite fluids, *Mathematika,* **20**, 175 (1973).
39. Singh, P., D.D. Joseph, J. Wang and R. Bai. Floating particles with sharp corners, in preparation (2003).
40. Singh, P., D.D. Joseph, T.I. Hesla, R. Glowinski & T.W. Pan. A distributed Lagrange multiplier/fictitious domain method for viscoelastic particulate flows, *J. Non-Newtonian Fluid Mech.* **91**, 165 (2000).
41. Singh, P. and L.G. Leal. Finite element simulation of the start-up problem for a viscoelastic problem in an eccentric cylinder geometry using third-order upwind scheme, *Theoret. Comput. Fluid Dynamics*, **5,** 107-137 (1993).

42. Sussman, M. An Adaptive Mesh Algorithm for Free Surface Flows in General Geometries, Adaptive Method of lines, Editors, A. Vande Wouwer, Ph. Saucez and W.E. Scheisser, Chapman and Hall/CRC, 207-227 (2001).
43. Sussman, M., P. Smereka & S. Osher. A level set approach for computing solutions to incompressible two-phase flow, *J. Comput. Phys.* **114**, 146 (1994).
44. Unverdi, S.O. & G. Tryggvason. A front-tracking method for viscous, incompressible, multi-fluid flows, *J. Comput. Phys.* **100**, 25 (1992).
45. Wakiya, S. Niigata Univ. College of Engng. Res. Rept. 6, Nagoaka, Japan (March 30, 1957).
46. Yan N. and J.H. Masliyah. Absorption and desorption of clay particles at the oil-water interface. *J. Colloid and Interface Science*, **168**, 386-392 (1994).

6. Figures

Figure 1. Neutrally buoyant glass beads cluster in water.

Figure 2. Spherical particles in water, (a) heavier-than-water hydrophobic particles. The meniscus between the particles is below the undisturbed level. Assuming that the contact angle remains fixed, the horizontal component of capillary force moves them toward each other. (b) Lighter-than-water hydrophilic particles will rise into the elevated section of the meniscus and come together.

Figure 3. Hydrophobic and hydrophilic particles in static equilibrium. The position of the contact ring determines the angle θ_C. The point of extension of the flat meniscus on the sphere determines the angle θ_1 .

Figure 4. For the contact angle $\alpha = 3\pi/4$, $\sin(\theta_c)\sin(\theta_c + \alpha)$ is plotted as a function of θ_C . Notice that the vertical component of interfacial force F_C given by (1) is negative for $\theta_C < \pi/4$ and maximum for $\theta_C \approx 1.9$.

Figure 5. (After Poynting and Thompson 1913). Horizontal forces associated with the fall (a) of liquid between hydrophobic plates and the rise (b) of liquid between hydrophilic plates. In (c) and (d) one plate is hydrophilic and the other hydrophobic. The contacts on both sides of a plate are the same and the tension γ is constant. They argue that the net horizontal force due to γ can be calculated at flat places; so that there is no net horizontal component of the tension. In (a) and (b) the pressures are such that they push the plates together; there is no net attractive force in (c). In (d) the plates are so close that there is no flat place, then the horizontal projection $\gamma \sin \alpha$ of the slope $\tan \alpha$ of the interface midway between the plates is smaller than the horizontal component γ outside the plates and the plate are pulled apart; they repel. They note that "…small bodies, such as straw or pieces of cork, floating on the surface of a liquid often attract each other in clusters; this occurs when the bodies are all wet by the liquid and also when none of them is wet; if one body is wet and one is not wet, they repel each other."

Figure 6. (a) A schematic of the interface shape and the contact line are shown for the initial and steady states. In simulations the contact angle on the particle surface is prescribed to be 135 degrees which is done by extending the level set function to the inside of particle. Notice that the contact line move downwards because of the interface deformation near the particle and this decreases the vertical component of interfacial tension force. (b) The unit normal to the particle surface, the tangent to contact line and the normal to the interface are shown.

Figure 7. The vertical component of velocity w for a particle released along the interface is shown as a function of time for three different values of the time step. The curve marked mesh B is for a more refined

mesh. The density and viscosity of the lower fluid are 1.0 gm/cm^3 and 1.0 Poise and that of the upper fluid are 0.1 gm/cm^3 and 0.1 Poise. The interfacial tension is 16.0 dynes/cm and the particle density is 1.05 gm/cm^3.

Figure 8. The particle position and the interface shape and the velocity field in the domain midsection are shown. 1—oblique view, 2—side view and 3—velocity field (a) t=0.003, (b) t=0.08.

Figure 9. The particle position and the corresponding interface shape are shown in the domain midsection. For the bottom circle and the interface shape the surface tension is 10 and for the top circle and the interface shape it is 25. The depth to which a particle sinks into the lower fluid decreases with increasing value of the surface tension.

Figure 10. The positions of two rigid particles suspended on the two-fluid interface and the velocity distribution at the domain midsection are shown at t=0.02, 0.59, 0.82 and 1.05. They are moving towards each other on the interface. Notice that the particles are "supported" by the capillary force which arises due to the deformation of the interface. The surface tension is 16.0 dynes/cm, the particle density is 1.01 g/cm^3 and the density of the top fluid is 0.1 g/cm^3 and that on the bottom is 1.0 g/cm^3. 1—oblique view, 2—velocity field.

Figure 11. The distance between the surfaces of particles and the approach velocity v2-v1 are plotted as functions of time. The approach velocity v2-v1 is shown for three different values of the time step. Notice that the approach velocity initially increases as the interface height between the particles decreases and then decreases as the gap between the particles becomes small.

Figure 12. The positions of four rigid particles suspended on the two-fluid interface are shown at t=0.02 and 0.96. They are moving towards each other on the interface. The surface tension is 16.0 dynes/cm, the particle density is 1.01 g/cm^3 and the density of the top fluid is 0.1 g/cm^3 and that on the bottom is 1.0 g/cm^3.

7. Tables

Table 1. The interfacial deformation h_2/R, the floating height $R\cos(\theta_c)$, the point of contact θ_c and the sum of the pressure and vertical component of interfacial forces obtained using (1) and (3) are shown as a function of the interfacial tension. The particle density is 1.05 and its weight is 4.315. The density of lower fluid is 1.0 and that of the upper fluid is 0.1. For all five cases, $F_p + F_c$ is approximately equal to the particle weight. Also notice that, as expected, the particle's floating height increases and the interface deformation decreases with increasing surface tension. The interfacial deformation in these calculations is restricted because the domain size is relatively small. But, we can still compare these values because the same domain is used in all calculations.

γ (CGS Units)	h_2/R	$R\cos(\theta_c)$	θ_c (degrees)	$F_p + F_c$ (g)
10	0.237	0.257	75.00	4.33
14	0.173	0.376	67.95	4.35
16	0.156	0.419	65.26	4.35
20	0.130	0.466	62.28	4.36
25	0.114	0.514	59.07	4.33

Table 2. The interfacial deformation h_2/R, the floating height $R\cos(\theta_c)$ and the point of contact θ_c are shown as a function of the upper fluid density. The interfacial tension is 16. The particle density is 1.05 and its weight is 4.315. The density of lower fluid is 1.0 and that of the upper fluid is varied. The particle's floating height increases and the interface deformation decreases with decreasing density of the upper fluid.

ρ_{upper} (g/cm^3)	h_2/R	$R\cos(\theta_c)$	θ_c (degrees)
0.1	0.156	0.419	65.26
0.01	0.159	0.417	65.34
0.0016	0.161	0.417	65.37

Table 3. The floating height $R\cos(\theta_c)$, the point of contact θ_c and the interfacial deformation h_2/R are shown as a function of the distance d between the particles. The interfacial tension is 16.0. The particle density is 1.05. The density of the lower fluid is 1.0 and that of the upper fluid is 0.1. Notice that the floating height of the particles decreases and the interfacial deformation increases as they come closer. These values should approach the values for an isolated particle when the distance d is large.

d (cm)	$R\cos(\theta_c)$	θ_c (degrees)	h_2/R
0.279	0.397	66.60	0.234
0.2493	0.388	67.13	0.289
0.2118	0.375	67.99	0.302

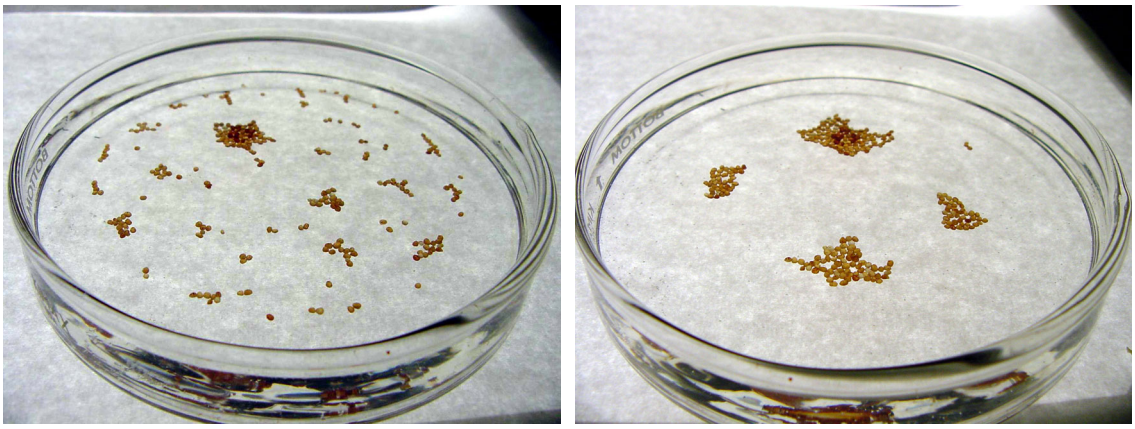

Figure 1. Neutrally buoyant glass beads cluster in water.

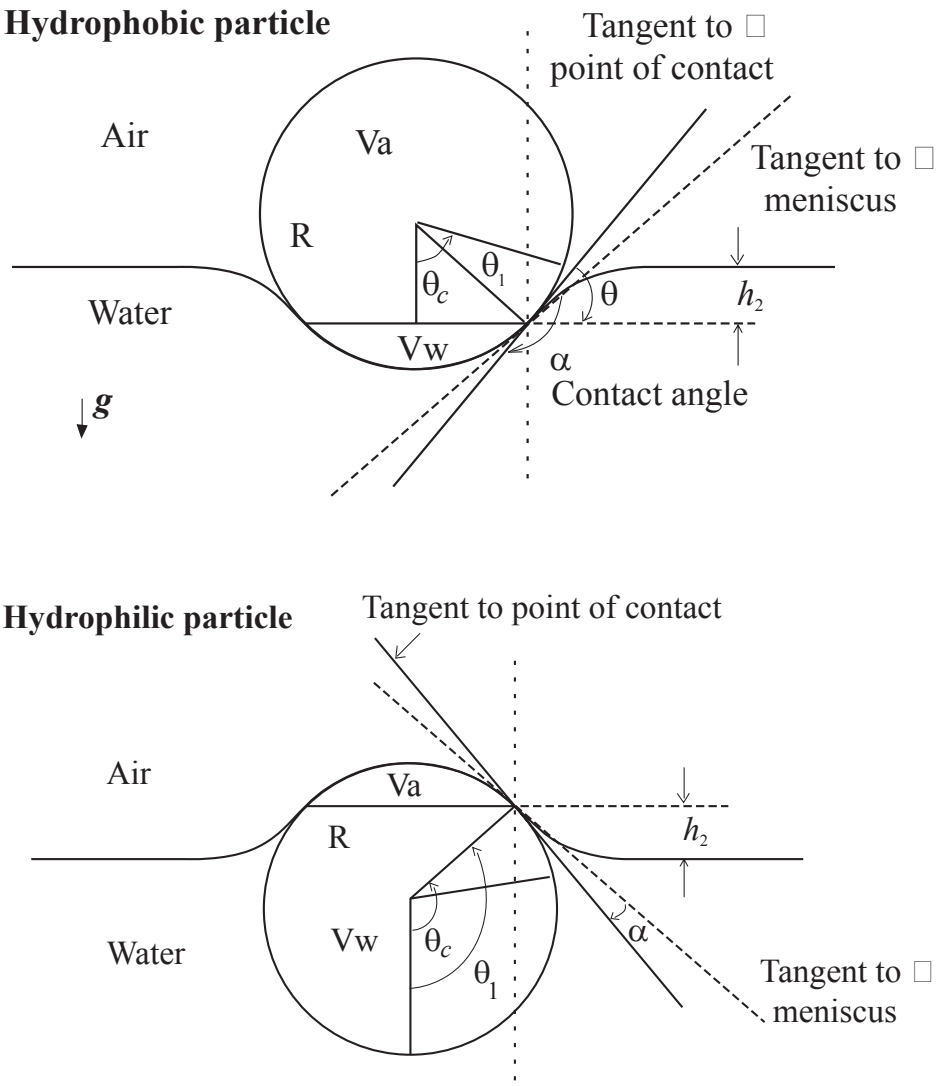

Figure 2. Hydrophobic and hydrophilic particles in static equilibrium. The position of the contact ring determines the angle θ_C. The point of extension of the flat meniscus on the sphere determines the angle θ_1 .

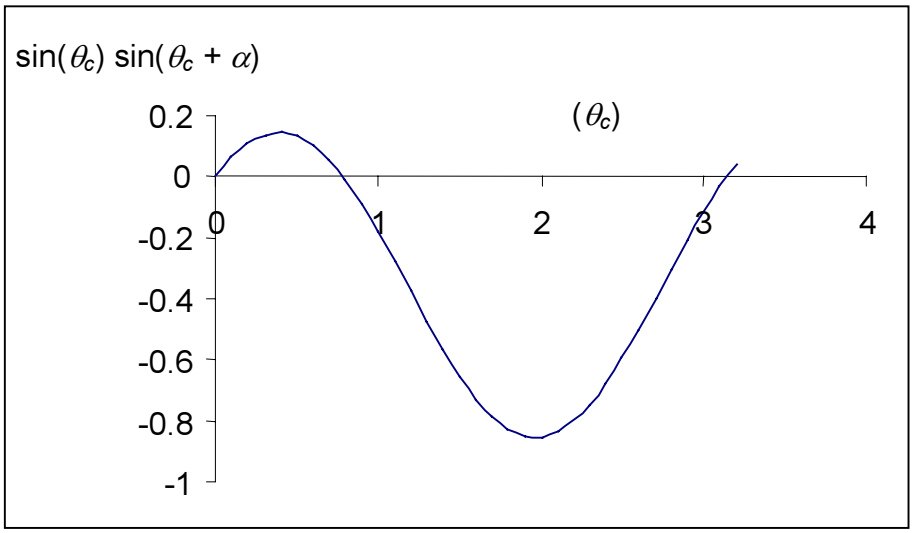

Figure 3. For the contact angle $\alpha = 3\pi/4$, $\sin(\theta_c)\sin(\theta_c + \alpha)$ is plotted as a function of θ_C. Notice that the vertical component of interfacial force F_C given by (1) is negative for $\theta_C < \pi/4$ and maximum for $\theta_C \approx 1.9$.

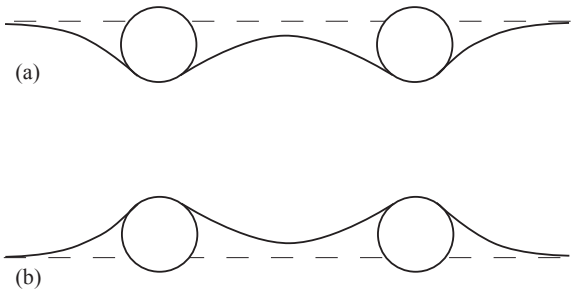

Figure 4. Spherical particles in water, (a) heavier-than-water hydrophobic particles. The meniscus between the particles is below the undisturbed level. Assuming that the contact angle remains fixed, the horizontal component of capillary force moves them toward each other. (b) Lighter-than-water hydrophilic particles will rise into the elevated section of the meniscus and come together.

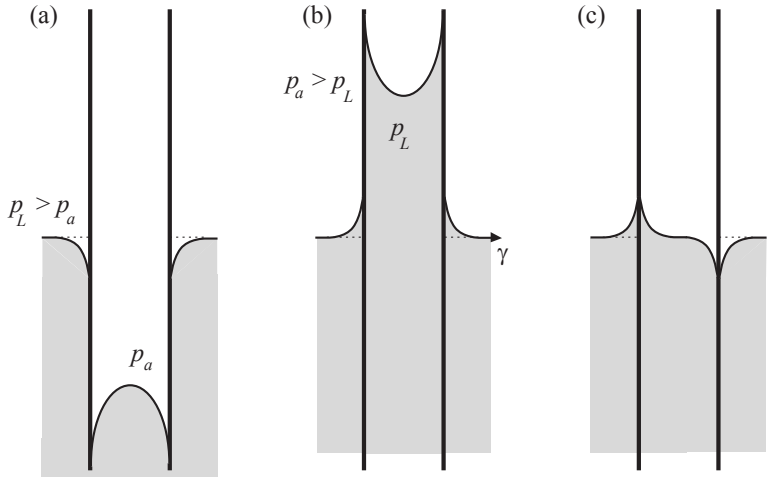

Figure 5. (After Poynting and Thompson 1913). Horizontal forces associated with the fall (a) of liquid between hydrophobic plates and the rise (b) of liquid between hydrophilic plates. In (c) one plate is hydrophilic and the other hydrophobic. The contacts on both sides of a plate are the same and the tension γ is constant. They argue that the net horizontal force due to γ can be calculated at flat places; so that there is no net horizontal component of the tension. In (a) and (b) the pressures are such that they push the plates together; there is no net attractive force in (c). If the plates (c) are so close that there is no flat place, then the horizontal projection γ sin α of the slope tan α of the interface midway between the plates is smaller than the horizontal component γ outside the plates and the plate are pulled apart; they repel. They note that "…small bodies, such as straw or pieces of cork, floating on the surface of a liquid often attract each other in clusters; this occurs when the bodies are all wet by the liquid and also when none of them is wet; if one body is wet and one is not wet, they repel each other." (It may help here to note that if one face of the plate is hydrophobic and the other hydrophilic, the contact angles will put the plates in tension, tending to pull them apart.)

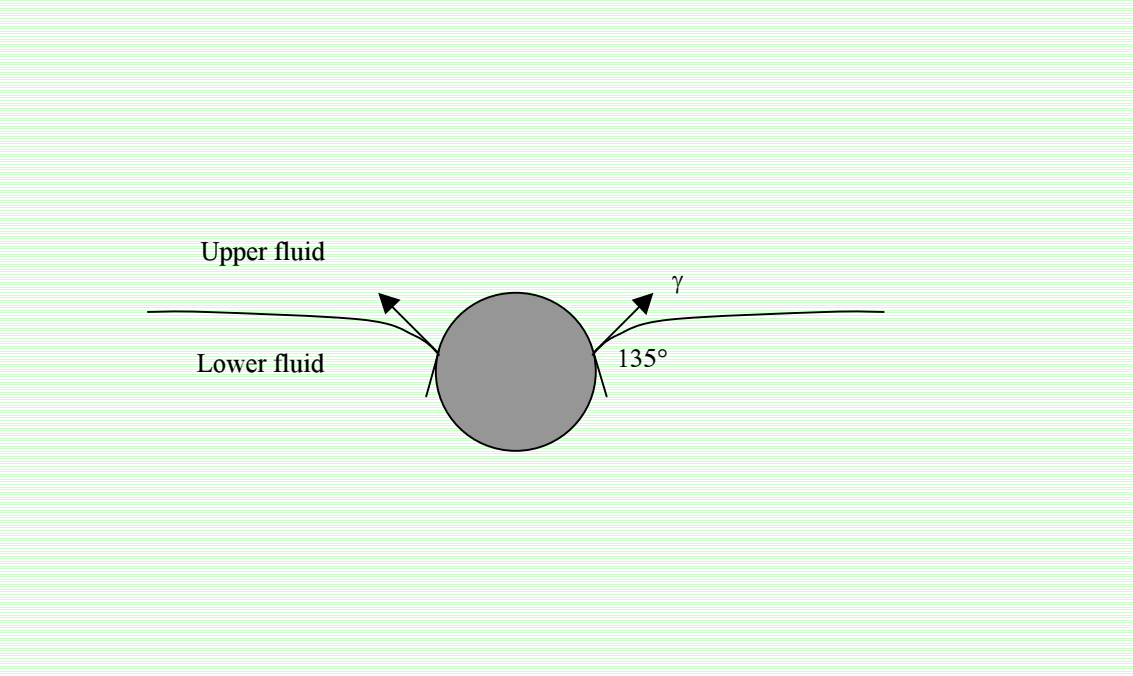

Figure 6. The contact angle on the particle surface is prescribed to be 135 degrees. This is done by extending the level set function to the inside of particle.

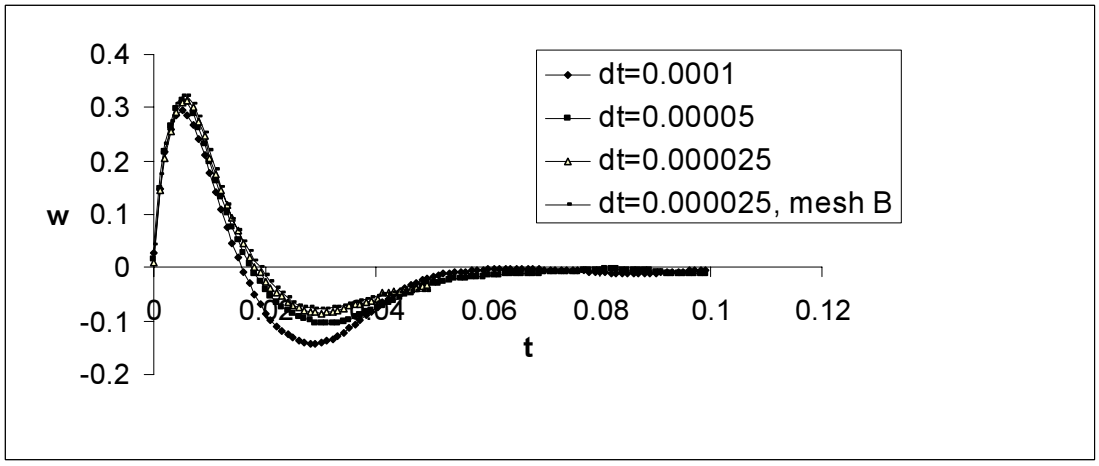

Figure 7. The vertical component of velocity w for a particle released along the interface is shown as a function of time for three different values of the time step. The curve marked mesh B is for a more refined mesh.

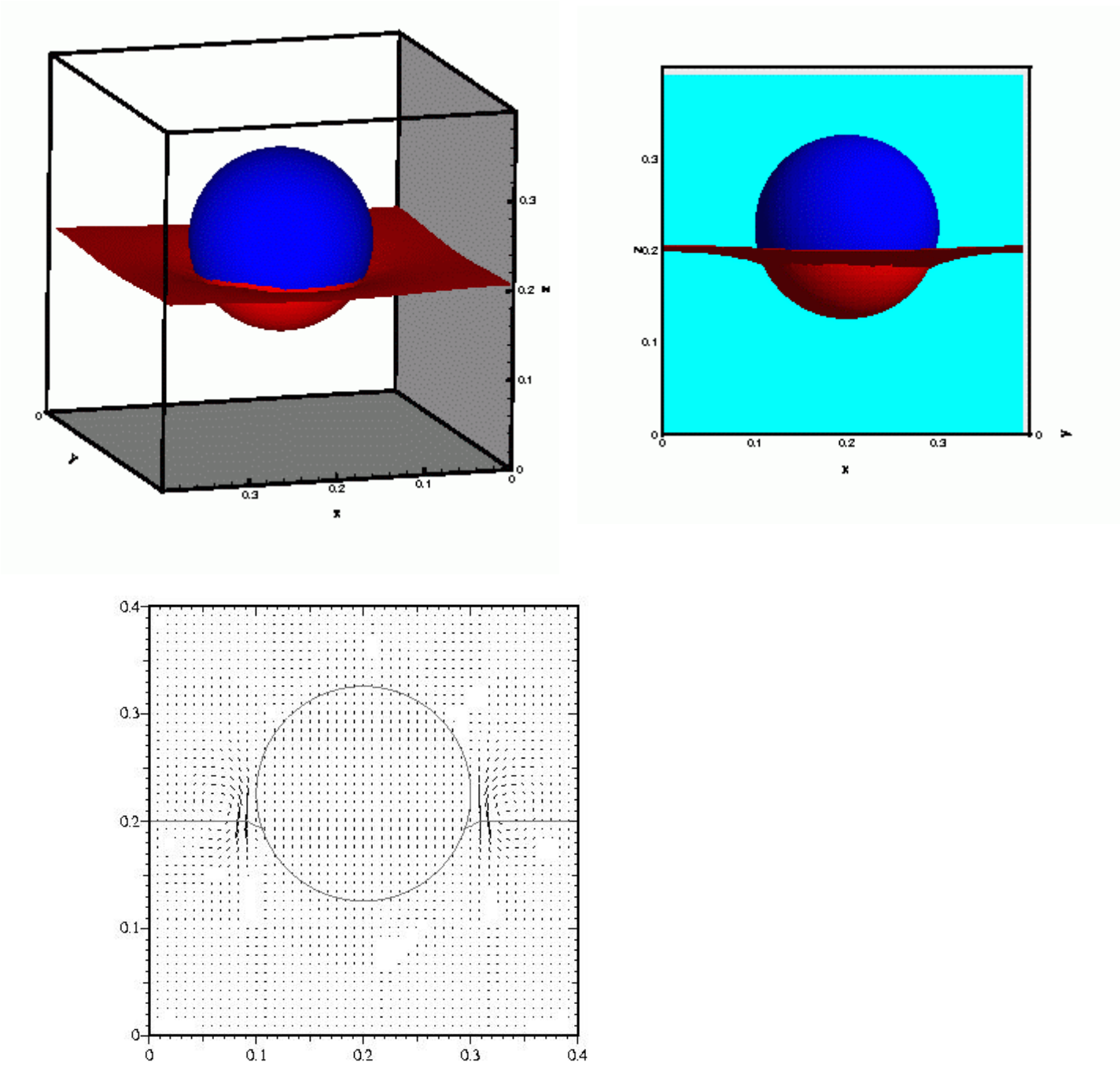

Figure 8. The particle position, the interface shape and the velocity field in the domain midsection are shown. (a) t=0.003 .

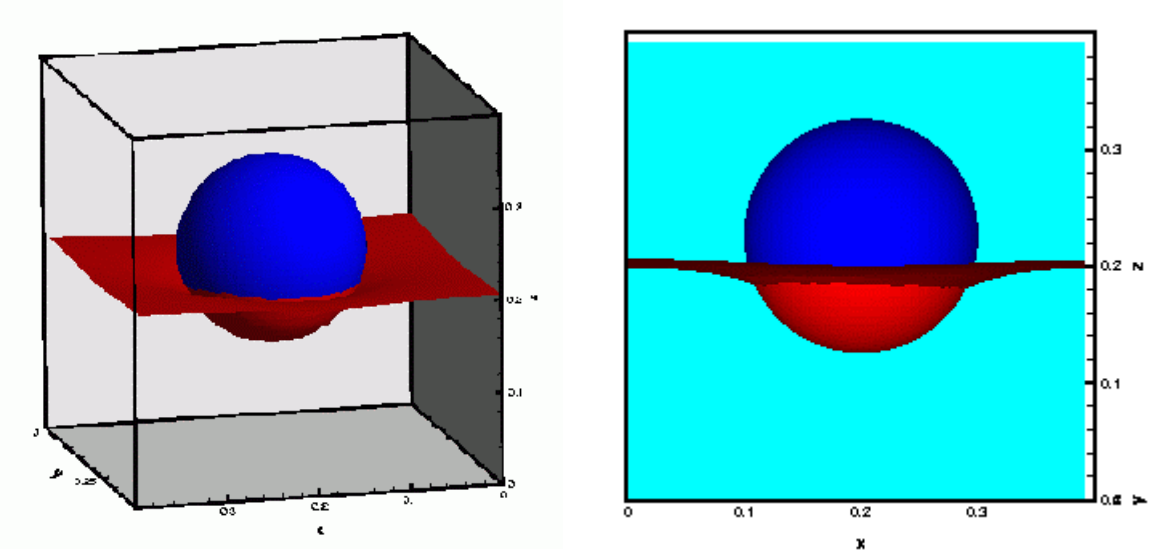

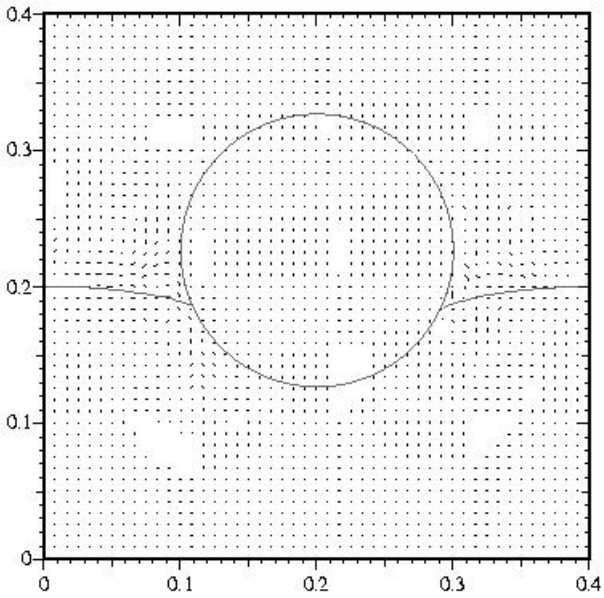

Figure 8b. t=0.08.

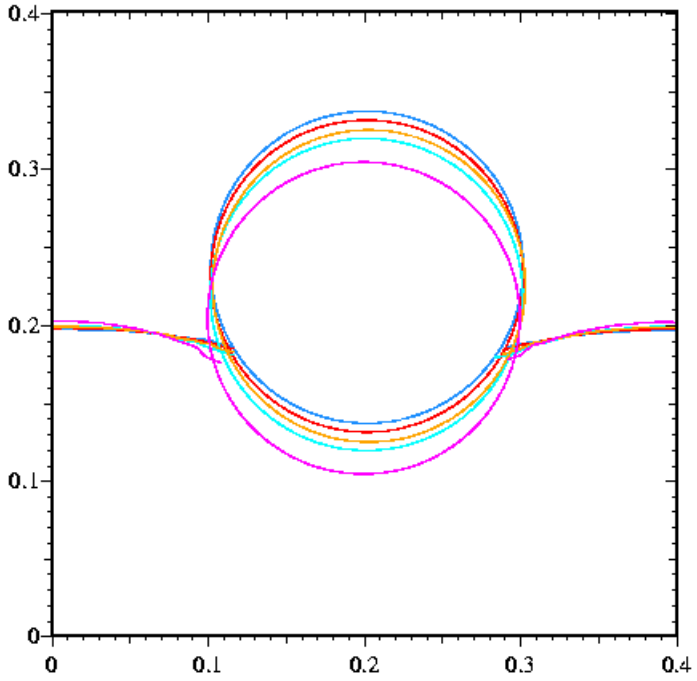

Figure 9. The particle position and the corresponding interface shape are shown in the domain midsection. For the bottom most circle and the interface shape the surface tension is 10 and for the top most circle and the interface shape it is 25. The other cases are for the surface tension values of 14, 16 and 20. The depth to which a particle sinks into the lower fluid decreases with increasing value of the surface tension.

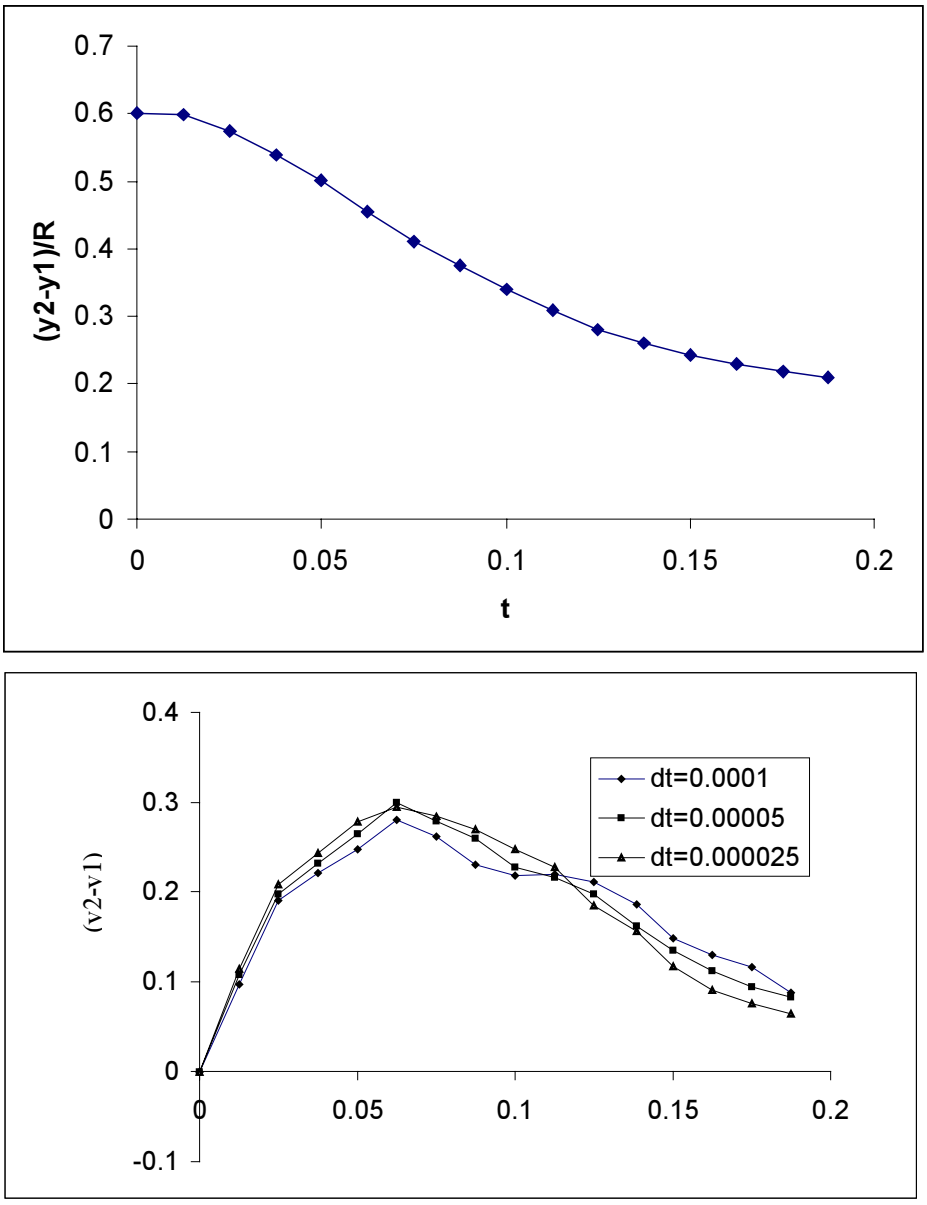

Figure 10. The distance between the surfaces of particles and the approach velocity v2-v1 are plotted as functions of time. The approach velocity w is shown for three different values of the time step. Notice that the approach velocity initially increases as the interface height between the particles decreases and then decreases as the gap between the particles becomes small.

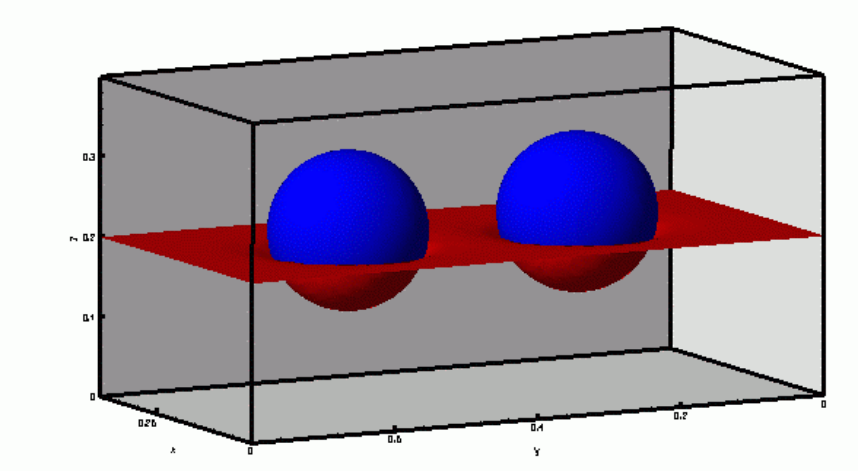
0.3
z 0.2
0.1
0
0.25
x
0
0.5
0.1
y
0.2
0

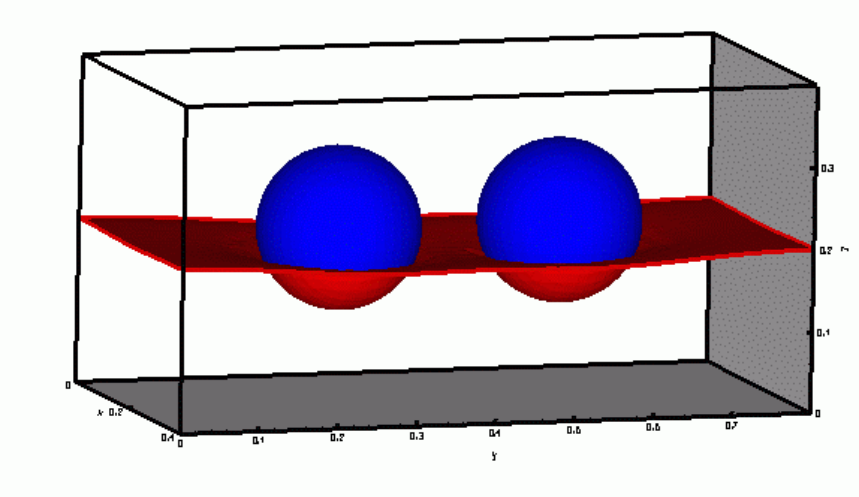
0.3
0.2 z
0.1
0
x 0.2
0.4
0
0.1
0.2
0.3
0.4
0.5
0.6
0.7
y

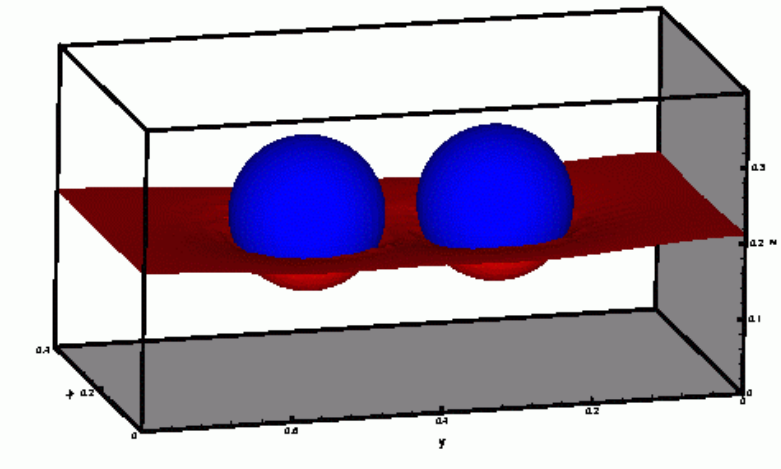
0.3
0.2 z
0.1
0
0.4
x 0.2
0
0.6
0.4
0.2
y

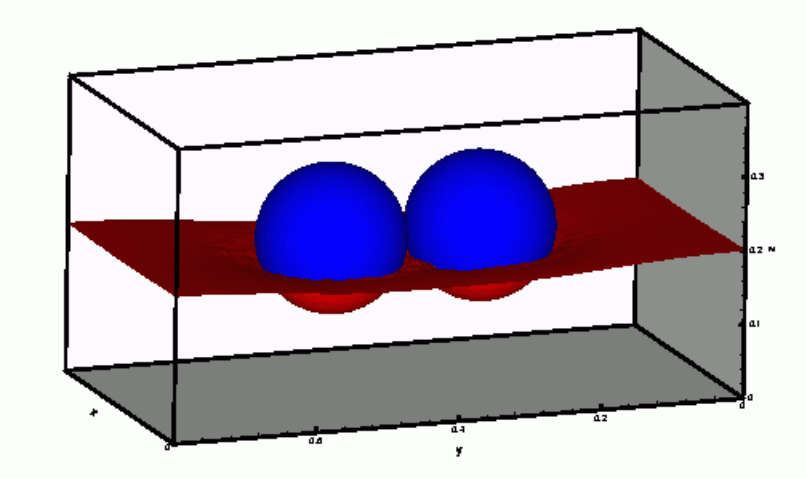

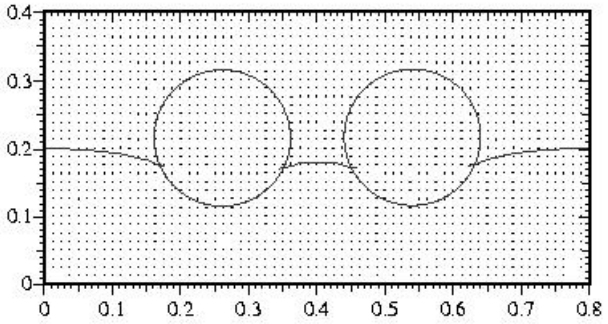
0.4
0.3
0.2
0.1
0
0
0.1
0.2
0.3
0.4
0.5
0.6
0.7
0.8

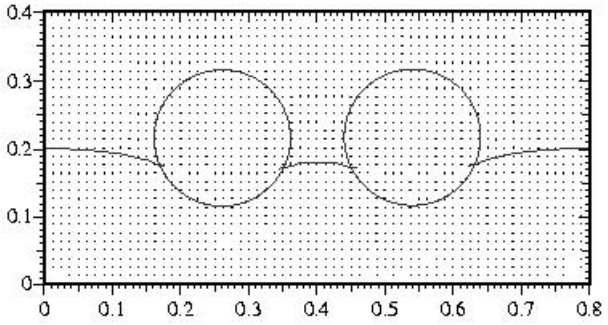
0.4
0.3
0.2
0.1
0
0
0.1
0.2
0.3
0.4
0.5
0.6
0.7
0.8

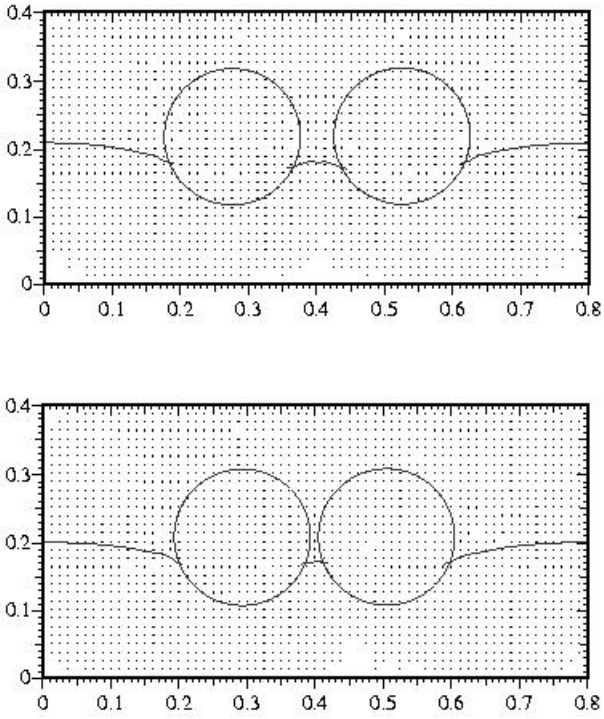

Figure 11. The positions of two rigid particles suspended on the two-fluid interface are shown at t=0.02, 0.59, 0.82 and 1.05. They are moving towards each other on the interface. Notice that the particles are "supported" by the capillary force which arises due to the deformation of the interface. The surface tension is 16.0 dynes/cm, the particle density is 1.01 g/cm^3 and the density of the top fluid is 0.1 g/cm^3 and that on the bottom is 1.0 g/cm^3.

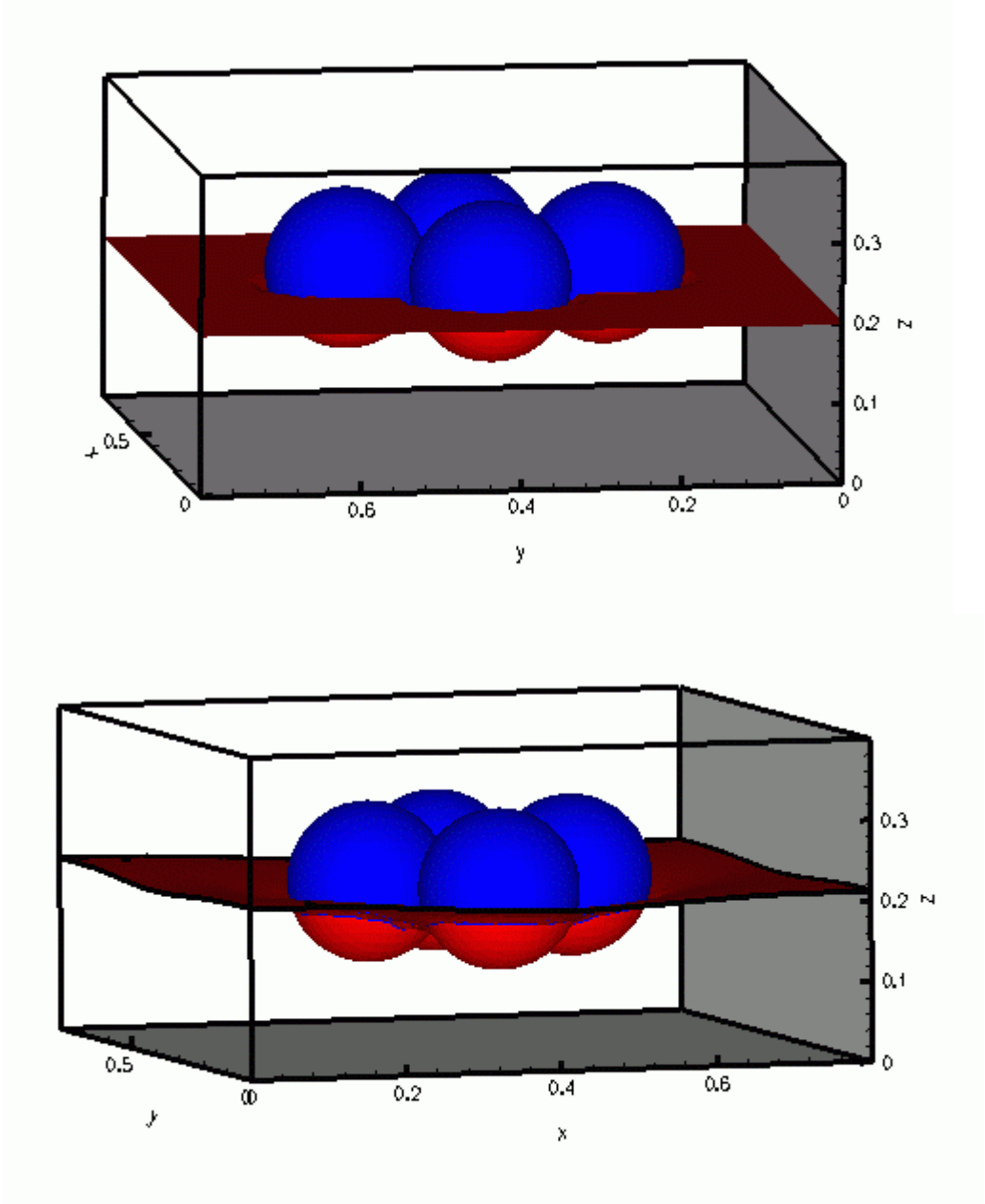

Figure 12. The positions of four rigid particles suspended on the two-fluid interface are shown at t=0.02 and 0.96. They are moving towards each other on the interface. The surface tension is 16.0 dynes/cm, the particle density is 1.01 g/cm^3 and the density of the top fluid is 0.1 g/cm^3 and that on the bottom is 1.0 g/cm^3.